

Unusual paraelectric system, KBr:Li^+

Robert John Russell*

*University of California, Santa Cruz, California 95064
and Carleton College, Northfield, Minnesota 55057*

Frank Bridges

University of California, Santa Cruz, California 95064

(Received 30 November 1981)

We have measured the paraelectric resonance absorption of lithium-doped KBr over the frequency range 42–217 GHz with electric fields applied along the $\langle 100 \rangle$, $\langle 111 \rangle$, and $\langle 110 \rangle$ orientations. Many lines are observed, with zero-field splittings (ZFS) ranging from 52 to 161 GHz for the ${}^7\text{Li}^+$ isotope. When ${}^6\text{Li}^+$ replaces ${}^7\text{Li}^+$, a large isotope shift of the ZFS (typically about 40%) is observed, indicating that Li^+ is tunneling in some multiwell potential. This paraelectric system is unusual in several respects: no significant changes in the relative line intensities are observed between 4.2 and 1.4 K, impurities such as OH^- can suppress the observed signal, and quenching low-concentration samples increases the signal intensity by factors of 10–1000. We attempted to fit the data to the standard tunneling models and had limited success with the $\langle 110 \rangle$ model; several (but not all) strong lines in each field orientation could be fit very well. However, when both the weak and strong lines are considered, too many ZFS are observed, which suggests that this Li^+ system is far too complex to be explained by any of the standard tunneling models. A comparison with other experiments and some suggestions for future work are included.

I. INTRODUCTION

Lithium-doped KBr forms a very unusual paraelectric-paraelastic system compared to other well-known paraelectric systems such as KCl:Li^+ .^{1,2} All early experiments^{3–6} provided little or no evidence for paraelectric behavior; consequently many investigators concluded that Li^+ occupies an on-center position in KBr. This argument appeared to be strengthened by far-infrared studies of both KCl:Li^+ and KBr:Li^+ .^{7–12} However, paraelectric resonance (PER) spectra, first presented in 1974,^{13,14} suggested that KBr:Li^+ is in fact a paraelectric system. Because of these strongly conflicting interpretations, a detailed PER study of KBr:Li^+ was undertaken using microwave frequencies over the range 40–215 GHz. In addition, many different sample preparations were tried and a series of diffusion experiments carried out both to characterize this system better as well as to understand why other experiments had given negative results. This paper is a detailed report of that work.

In Sec. II, we give a brief review of the usual tunneling models used to describe paraelectric systems as well as discuss briefly some additional pos-

sibilities which involve a second impurity. Calculations of the effective potential which determines whether the defect is on or off center are also reviewed. In Sec. III we discuss some of the experimental details, including the high-frequency spectrometer and some of the sample-preparation procedures. The new experimental results are presented in Sec. IV and are analyzed in Sec. V. Section VI reviews the earlier works and discusses them in light of this comprehensive PER investigation. Our final conclusions are summarized in Sec. VII.

II. THEORETICAL BACKGROUND

A. Paraelectric models

Most off-center paraelectric systems (e.g., KCl:Li^+ , RbCl:Ag^+) have been analyzed using tunneling models discussed by Gomez *et al.*,¹⁵ Shore,¹⁶ and Sauer *et al.*¹⁷ Here we present the models briefly and introduce the experimental parameters which are usually used to characterize the data.

Consider n equivalent potential wells arranged about a lattice site in a manner consistent with the

symmetry of the host crystal. Each well represents an off-center position of the ion and for the cubic systems, the three simplest models have six, eight, and 12 potential wells in the $\langle 100 \rangle$, $\langle 111 \rangle$, and $\langle 110 \rangle$ directions, respectively. In the limit of infinite barriers between wells, an ion in one of the wells is isolated from all the other wells, and the ground-state energy is n -fold degenerate. Since the potential barriers are in fact finite, tunneling can occur between wells, typically at microwave frequencies. This coupling between wells lifts the n -fold degeneracy producing a ground-state multiplet of closely spaced energy levels, with each level being at most threefold degenerate.

Such a coupling is parameterized by introducing off-diagonal tunneling elements of the form $\langle i | H_c | j \rangle$ where $|i\rangle$ represents a *directed* state localized in well i , and H_c is the defect Hamiltonian which includes both the crystal field and defect kinetic energy. For systems of cubic symmetry such as the alkali-halide crystals, only a few distinct parameters are needed. Using the notation of Gomez *et al.*,¹⁵ two tunneling parameters, representing tunneling between nearest and next-nearest neighbors, are needed for the $\langle 100 \rangle$ system (denoted by η and μ). For the $\langle 111 \rangle$ system third-nearest-neighbor tunneling (denoted by ν) can occur, and in the most complicated dipole system, the $\langle 110 \rangle$ model, fourth-nearest-neighbor tunneling is also possible (denoted by σ). By using finite-group theory, the tunneling matrix H_c is easily diagonalized and the tunneling eigenstates and eigenvalues are obtained.¹⁵

If a dc electric field \vec{E}_{dc} is now applied, an additional interaction $-\vec{p}^{(i)} \cdot \vec{E}_{dc}$ must be included for each potential well,^{2,15} where $\vec{p}^{(i)}$ is the dipole moment of the ion in the i th well. This further splits the energy levels of the ground-state multiplet, and in the high-field limit the levels shift linearly with field.

The order of the zero-field energy levels depends on the signs and magnitudes of the tunneling parameters. In general, there is no unique connection between these "zero-field" states and the states obtained in the presence of a large electric field. In the preceding paper,¹⁸ the various connections and a systematic method for comparing the data to the resulting theoretical spectra is given. In these calculations, the A_{1g} state is assumed to be the lowest-energy state, but the usual restriction that all tunneling elements be negative, is lifted.

Transitions between these energy levels can be induced by a high-frequency ac electric field applied either parallel or perpendicular to the dc elec-

tric field with frequencies typically ranging from several GHz to several hundred GHz. The matrix elements for such PER transitions depend on the magnitudes of the various tunneling parameters and, depending on which parameters are important and the field orientation, several resonance lines may be observed. Usually these resonances are investigated by measuring the microwave power absorption as a function of electric field for a series of fixed frequencies.

B. Theoretical model for off-center behavior

The prediction of off-center behavior has been a difficult and challenging problem for many years. The basic physical idea is quite simple: When the overlap repulsion forces experienced by an impurity ion are smaller than the polarization forces, the ion moves to an off-center position. However, the difference in the corresponding repulsive and polarization energies is very small and is consequently extremely sensitive to small details of the proposed models. Early work by Quigley and Das¹⁹ and Wilson *et al.*²⁰ all agree upon an off-center position for KCl:Li⁺ but differ for KBr:Li⁺. This latter system appears in theory to be a borderline case between on- and off-center behavior.

In 1978 Catlow *et al.*²¹ reconsidered this problem using new potentials based on the shell model. With the form of the potential that gives well-defined $\langle 111 \rangle$ off-center positions for KCl:Li⁺, they find a weakly off-center system for KBr:Li⁺—the central barrier being so low that well-defined off-center localized states are not predicted by this model.

In a tabulation of the off-center energies of Li⁺ in alkali-halide host crystals by Catlow *et al.*,²¹ several trends appear. First, increasing the size of the host alkali-metal ion leads to deeper off-center wells. This is as expected, since the overlap repulsion term should decrease when the cation vacancy is larger. Second, off-center displacement becomes less likely as the anion size is increased. This is in contrast to the experimental situation²² for Cu⁺ and Ag⁺ ions, for which an increase in the host-anion size leads to deeper off-center minima.

Finally, in a very recent calculation, using the method of Catlow *et al.*²¹ but different potentials, Sangster²³ obtained $\langle 111 \rangle$ off-center behavior for KBr:Li⁺. Thus the theoretical status for off-center behavior of Li⁺ in KBr is far from clear.

C. Other models

Because of the negative results (see Sec. VI B) in many other experiments,³⁻¹² we have also considered several models in which the off-center position of the Li^+ ion arises solely because of the presence of a second impurity at a nearby site. The concentration of such complexes is expected to be considerably less than the Li^+ concentration unless Li^+ ions can easily be trapped by other impurities. If such a model were found that was consistent with the PER data, it might explain the negative results from other, less sensitive, techniques. We compare such models with our data in Sec. V.

On the other hand, we do not consider the case of two interacting *off-center* ions which are on second-nearest-neighbor sites. Such ions should also exhibit isolated off-center behavior, and with the concentrations and the sample preparation used (Sec. III B), the isolated ions are expected to dominate the PER spectra. We also do not include here more complicated single-ion paraelectric models which are consistent with O_h symmetry, such as a set of 24 equivalent wells.

1. Tunneling models with a single plane of potential wells

a. $\text{Li}^+:\text{X}^-$. In the simplest models we assume that some additional negative-ion impurity (X^-) is present at the nearest-neighbor anion site, producing a C_{4v} axis in the crystal. Here, and in the cases which follow, one must of course consider a uniform distribution of such C_{4v} axes throughout the sample. As a result of the X^- impurity, the Li^+ ion may go off center in a manner consistent with the C_{4v} symmetry, and in the simplest case, it would tunnel in a plane perpendicular to the C_{4v} axis. Two different complexes might occur: (i) The Li^+ may be off center along the four $\langle 100 \rangle$ directions, or (ii) it may be off center along the four $\langle 110 \rangle$ directions. The details of this model are outlined in Appendix A 1.

b. $\text{Li}^+:\text{Y}^+$. Here we consider a positive ion (Y^+) which lies at a second-nearest-neighbor site along a $\langle 110 \rangle$ crystal axis. This axis has C_{2v} symmetry and an off-center impurity with this symmetry would have either two or four potential wells perpendicular to the C_{2v} axis: (i) along two $\langle 100 \rangle$ directions, (ii) along two $\langle 110 \rangle$ directions, or (iii) along four $\langle 111 \rangle$ directions. The details are given in Appendix A 2.

One special case of this complex, that obtained

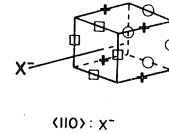


FIG. 1. Example of an off-center system induced by a nearest-neighbor impurity ion X^- . Different off-center positions are indicated by circles, squares, and crosses. These three groups of potential wells are not equivalent, and the ground-state energies are assumed to be split by energies ϵ_1 and ϵ_2 (see Appendix A).

when Y^+ is in fact a second Li^+ ion, deserves further comment. In this case, both Li^+ ions would be off center and the axis is D_{2h} if the $\text{Li}^+:\text{Li}^+$ pair tunnel together. If one wishes to allow each Li^+ to tunnel independently, then the symmetry is even lower.

2. Tunneling models with several inequivalent planes of potential wells

In this case, we assume that the lithium ion is forced off center in more than one plane as suggested in Fig. 1. We consider sets of planes with a common axis of C_{4v} symmetry, and with tunneling between planes still allowed. The complete set of possible off-axis positions in each case can be seen to display cubic symmetry, much like the $\langle 100 \rangle$, $\langle 111 \rangle$, and $\langle 110 \rangle$ geometries. However, in these cases we assume that the C_{4v} interaction dominates such that the *energy separation of the tunneling planes is much greater than the tunneling parameters*. We also assume for simplicity that the off-center displacement, and hence the dipole moment, is relatively independent of the X^- impurity interaction.

a. $\langle 100 \rangle:\text{X}^-$ model. If lithium is forced off center along the $\langle 100 \rangle$ directions by a second impurity we find (Appendix A 3 i) that (1) backward lines (lines that move to lower E field when the frequency is increased) occur for either η or μ dominant, and that (2) for $\vec{E} \parallel \langle 111 \rangle$ only one slope should be observed.

b. $\langle 111 \rangle:\text{X}^-$ model. If the lithium is off center along the $\langle 111 \rangle$ directions (Appendix A 3 ii), then (1) backward lines occur for any choice of dominant tunneling parameter, and (2) for $\vec{E} \parallel \langle 100 \rangle$, a single slope should be observed.

c. $\langle 110 \rangle:\text{X}^-$ model. This model is similar to the above two cases (Appendix A 3 iii). The most important feature is that for any choice of dominant tunneling parameter(s), backward lines should occur for both $\vec{E} \parallel \langle 100 \rangle$ and $\langle 111 \rangle$.

III. EXPERIMENTAL APPARATUS AND SAMPLE PREPARATION

A. Microwave spectrometer

In paraelectric spectroscopy, resonant absorption transitions are induced between electric-field-dependent energy levels by irradiating the sample at liquid-helium temperatures with microwave radiation. For frequencies below 75 GHz a reflection spectrometer was used.²⁴ Preliminary PER data¹³ on KBr:Li⁺ showed unusually high zero-field splittings (ZFS) up to 65 GHz. Both to search for even higher ZFS, and to follow the newly discovered lines to higher fields, our spectrometer was extended to higher frequencies using second-harmonic generation. The resulting transmission spectrometer²⁵ initially provided data up to 150 GHz for electric fields up to 150 kV/cm. The discovery¹⁴ of yet another ZFS at 140 GHz necessitated a second extension to third-harmonic frequencies. Normally the power was down by an additional 10–20 dB below second harmonic, but still provided reasonable data.

This work required a smaller cavity, since the mode spacing decreases rapidly with increasing frequency. The cavity was spark-cut from brass ($1.3 \times 1.0 \times 0.50 \text{ cm}^3$) and after indium coating, it exhibited quite reasonable Q 's (2000–3000) for many modes at second- and third-harmonic frequencies.

A third-harmonic filter was also designed, $0.015 \times 0.102 \text{ cm}^2$ in cross section and 1.9 cm in length. Tapered transition sections matched the reduced rectangular waveguide to standard RG98/U, so that the existing head could be used.

B. Sample preparation

Most of our boules were grown at the Crystal Growth Facilities of the University of Utah in Salt Lake City. One boule of KBr:⁶Li⁺ came from Cornell. They were usually grown to a specified dopant concentration in the melt; however some boules were prepared partially doped, leaving a pure end. The boules were initially aligned by x-ray diffraction along either the $\langle 100 \rangle$, $\langle 111 \rangle$, or $\langle 110 \rangle$ orientations, and slices taken using a string saw and water. After more careful alignment to within 0.5° , samples were cut (or cleaved) from the slice and then lapped to the desired thickness. Thicknesses ranged from 0.03 to 0.09 cm.

Most of our samples were taken from the doped

portion of the boules. Others, cut from the pure end, were run to check for the presence of signals in the starting material. In addition, we also prepared samples by diffusing LiBr into pure material. Normally a $5\text{-}\mu\text{l}$ droplet of LiBr solution was placed on the sample surface and immediately evaporated by an air gun leaving a fine uniform layer of dopant material on the surface. The sample was then placed in a nitrogen atmosphere and heated to the desired temperature. For some samples, we used KBr and LiBr which had been specially prepared to remove OH⁻. In this case, we sprinkled the *powdered* LiBr onto a sample inside a glove box, prior to diffusion.

Preliminary measurements showed that one hour at temperatures of 400–450°C gave quite reasonable results. We also checked roughly how far the lithium had diffused into one sample by measuring the change in the intensity of the PER signal after part of the doped side of the sample was lapped off. In this case, the lithium had diffused less than half-way through the sample.

In one series of experiments we wanted to measure the concentration dependence of the PER signal, using the same host material. This was achieved by using identical samples cut from the same pure KBr crystal, and adding Li⁺ via diffusion. To control the concentration of Li⁺ we prepared a set of LiBr solutions with Li⁺ concentrations in the ratio 10:25:50:200. In each case we used $5 \mu\text{l}$ and diffused each sample at 450°C for 1 h. These samples were cooled slowly to room temperature (several hours) and run without lapping the doped surface.

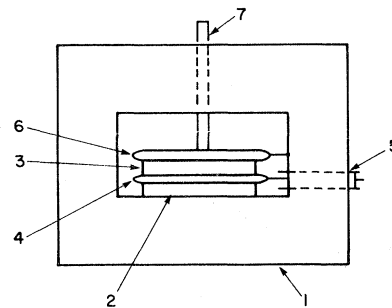


FIG. 2. Experimental arrangement for measuring the intensity of the KBr:Li⁺ signal relative to a calibration sample of KCl:Li⁺. Thickness of the latter was chosen so that the calibration signal did not overlap the KBr signal. 1—cavity body, 2 and 3—KBr and KCl samples, 4—high-voltage electrode, 5—Mylar-insulated high-voltage feed-through, 6—ground electrode connected to cavity body, 7—spring-loaded quartz pushrod to hold samples in place.

The relative signal intensity was obtained by comparing the $\text{KBr}:\text{Li}^+$ signal to that of a $\text{KCl}:\text{Li}^+$ reference crystal mounted above the KBr sample (Fig. 2). For each sample the intensity ratio was measured at several different frequencies and the average taken. Interchanging the sample and reference crystals gave the same results.

Several other diffusion experiments were also carried out. First F^- , Cl^- , Na^+ , O^{2-} , and H^+ were each diffused into pure KBr samples to check for any PER signal from these impurities. Then, after a preliminary experiment suggested that OH^- in some way influences the observed PER spectra, we carried out several diffusion experiments involving both Li^+ and OH^- ions. For the F^- , Cl^- , Na^+ , and OH^- ions, a uniform layer of dopant material (KF , KCl , NaBr , and KOH , respectively) was placed on one side of the sample following the same technique used for Li^+ . For O^{2-} and H^+ , the sample was heated to 450°C in an O_2 or H_2 atmosphere.

Several heat treatments were used on both the melt-doped and diffusion-doped samples. In some cases we quenched the samples by raising them to high temperatures (650°C) for approximately 10 min, and then cooling them rapidly to room temperature in less than 2 min. Other samples were annealed to remove strains by lowering the temperature slowly over 10–12 h.

Lithium concentrations for a few of the melt-doped boules were measured using a Varian Techtron atomic absorption spectrophotometer. Also one boule was doped with U centers so that F centers [and $F_A(\text{Li}^+)$ centers] could be produced. Details are provided in Table I.

IV. DATA PRESENTATION

Our data consist of swept-field traces taken at fixed frequencies, in which we record the derivative line shape of the resonance absorption signal. Some scatter is inevitable due to variations from sample to sample, the widths of the lines, as well as the partial overlap of multiple resonances. Although in some cases, broad lines were narrowed by annealing the sample, most factors which contribute to the linewidth—inhomogeneous strain broadening, internal inhomogeneous electric fields, and tunnel dressing—could not be eliminated. Except near a ZFS, one can reliably estimate the relative intensities of two well-separated lines by measuring the ratio of the product of their heights times the square of their widths, using peak-to-peak values for widths and heights. The relative

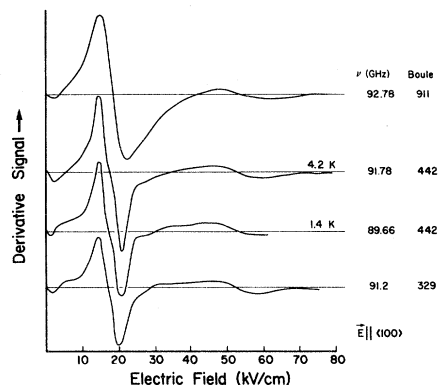


FIG. 3. Several traces for $\text{KBr}:\text{Li}^+$ at frequencies near 92 GHz with $\vec{E} \parallel \langle 100 \rangle$. Boules 442 and 329 are melt doped while boule 911 is diffusion doped. Traces have been replotted to give the same peak-to-peak heights of the main line. Spectra obtained for different boules and for both melt- and diffusion-doped samples are the same. All traces are for $T=4.2$ K except one trace for boule 442 taken at 1.4 K.

intensities of poorly resolved lines depends, of course, on the actual decomposition, but in many cases it could be estimated to within a factor of 2.

A. Presentation of the $^7\text{Li}^+$ data

Much of the $^7\text{Li}^+$ data was taken using boules 442, 329, and 911. Boule 442 was used for both melt-doped and diffusion-doped samples. The pure end of boule 911 was also used for diffusion-doped samples. Boule 329 included U centers in its preparation, but gave the same signal. A few samples from boules 602 (quenched), 1014 (diffusion doped), and 1142 were used to spot check the spectrum at various frequencies.

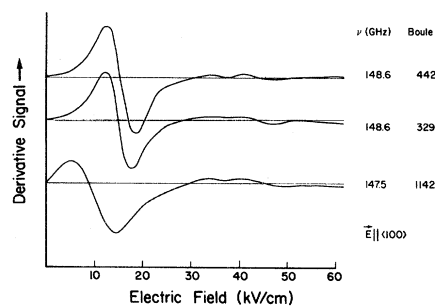


FIG. 4. Several traces for $\text{KBr}:\text{Li}^+$ at frequencies near 148 GHz for $\vec{E} \parallel \langle 100 \rangle$. All samples are melt doped and all traces taken at 4.2 K. Traces have been replotted to give the same peak-to-peak heights.

TABLE I. KBr crystals doped with Li⁺.

Boule No.	Melt concentration/ estimated concentration	Measured concentration	Pure end?	Comments
⁷ Li ⁺ 329	8 × 10 ⁻³ /350 ppm		No	Strong Li ⁺ signal, <i>U</i> centers present
442	5 × 10 ⁻³ /220 ppm	375 ppm	Yes	Strong Li ⁺ signal, both melt doped and diffusion doped
475	5 × 10 ⁻⁵ /2 ppm		No	No signal, even after heat treat- ment
493	5 × 10 ⁻⁴ /22 ppm		No	No signal at first, Li ⁺ signal present after quenching
602	10 ⁻³ /44 ppm	65–75 ppm	Yes	Li ⁺ signal, plus anomalous signal which disappeared after quenching, leaving strong Li ⁺ signal
911			Yes	Undoped end of KBr:F ⁻ crystal; strong Li ⁺ signal after Li ⁺ diffusion
1014	Pure		Yes	Treated to remove OH ⁻ ; strong Li ⁺ signal from quenched, diffusion-doped samples
1142	8 × 10 ⁻³ /350 ppm		Yes	Strong Li ⁺ signal
⁶ Li ⁺ 949	8 × 10 ⁻⁴ /35 ppm		No	Strong Li ⁺ signal
1143	8 × 10 ⁻³ /350 ppm		Yes	Strong Li ⁺ signal
Cornell (7 206 204W)	5 × 10 ⁻³ /220 ppm		No	Strong Li ⁺ signal

In Figs. 3 and 4, we show several typical traces (the derivatives of the absorption line) at frequencies near 92 and 148 GHz for samples of KBr:⁷Li⁺ from boules 329, 442, 622, 911, and 1142. Except for one trace (boule 442) in Fig. 3, all data is for 4.2 K. The relative integrated intensities of all the well-defined lines are the same in each boule to within 50%. Higher accuracy in the intensity measurements is difficult to achieve because the lines often overlap. Broadening effects are also clearly present. In Fig. 3 the traces for boule 442 suggest that the strongest line is a sum

of two lines with a weaker line at a slightly higher electric field. The trace for boule 329 is also suggestive of such a composition. However, the first trace (diffusion-doped boule 911) shows a broader line in which these details are no longer visible. Otherwise, the diffusion-doped samples exhibit the same spectra as the melt-doped samples.

Figure 4 shows another effect that results from broadening interactions—an apparent shift of the center of the line to lower frequencies plus a less symmetric line shape²⁶ for resonances at low electric fields. The trace for boule 1142 shows this ef-

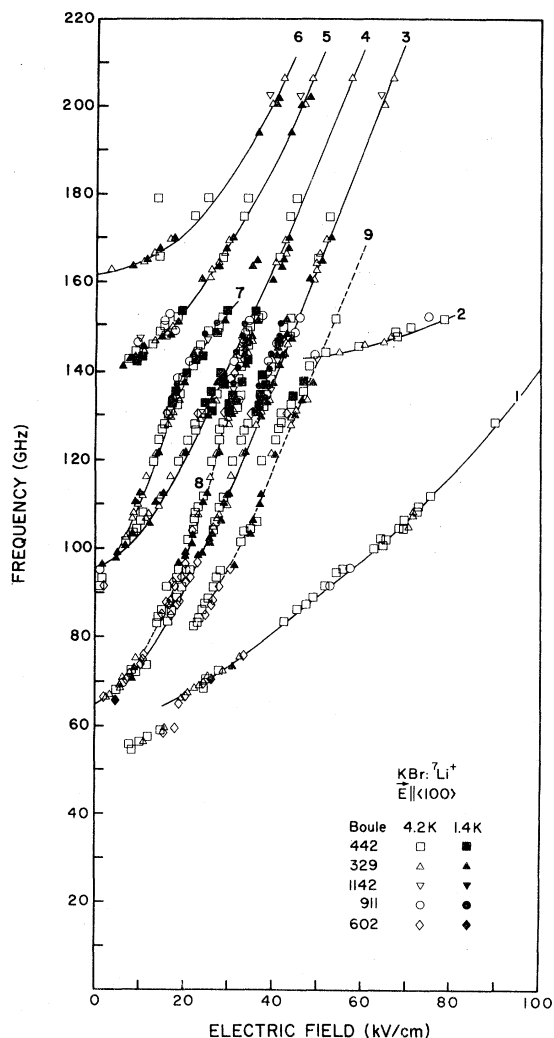


FIG. 5. Plot of the line position as a function of electric field with $\vec{E} \parallel \langle 100 \rangle$ for samples taken from several different KBr boules doped with ${}^7\text{Li}^+$. Open symbols are for $T = 4.2$ K and solid symbols are for $T \approx 1.3$ K. Not all points are included in this and the following composite graphs. In this and the following figures solid lines represent strong absorption lines and dotted lines represent weak absorption lines.

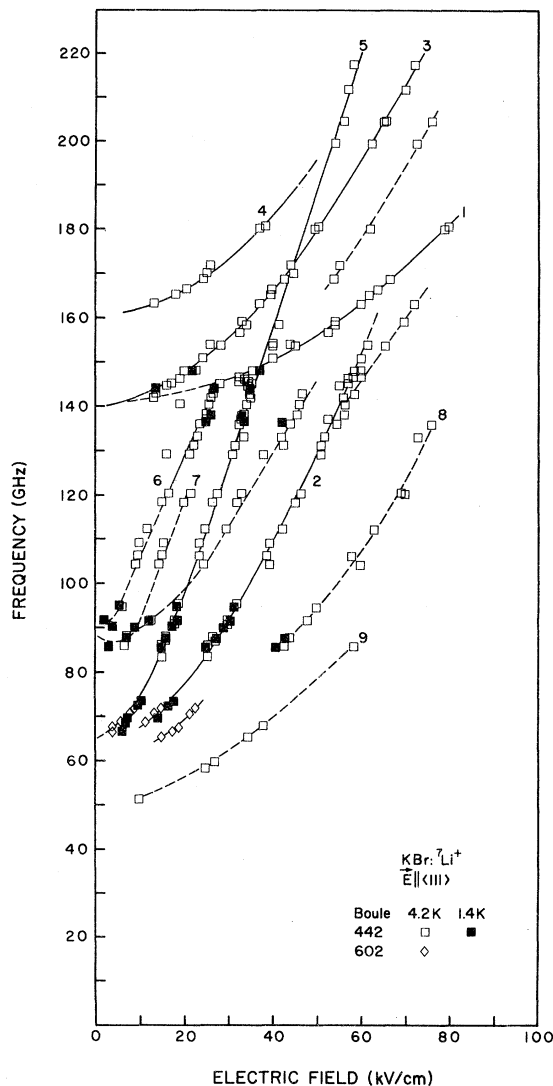


FIG. 6. Plot of the line position as a function of electric field with $\vec{E} \parallel \langle 111 \rangle$ for samples taken from several different KBr boules doped with ${}^7\text{Li}^+$. Open symbols are for $T = 4.2$ K and solid symbols are for $T \approx 1.3$ K.

fect quite clearly.

In Figures 5, 6, and 7 we show the composite of data taken from several boules for $\vec{E}_{dc} \parallel \langle 100 \rangle$, $\langle 111 \rangle$, and $\langle 110 \rangle$, respectively. Approximately 20 samples are represented in these traces, and the composites show *striking* overall consistency. In each figure, we have used a *solid line to indicate the stronger transitions, and dashed lines to show weaker transitions*. (These curves are purely a guide to the eye.) We have numbered the lines for

easy identification but occasionally refer to lines by their ZFS.

For the $\langle 100 \rangle$ orientation (Fig. 5) the six strongest lines occur in two groups: with high slopes and low slopes. Four high-slope lines (3, 4, 5, and 6) have clear ZFS's at 65, 95, 140, and 161 GHz. Lines 5 and 6, though still turning over at the limit of the frequency domain, do seem to be approaching the same high-field slope as line 3. The 65- and 95-GHz ZFS's are unusual in that they each

form doublets. The upper line in each case is weaker, has a higher slope, and appears to have more structure than the rest of the lines. The two low-slope lines at 60–65 and 140 GHz (lines 1 and 2) show nonlinear behavior over the range of fields used, but may be approaching a slope half that of the high-slope lines. There is evidence, though limited, for a still lower ZFS near 52 ± 3 GHz. The strong lines, in order of decreasing strength, are: 2, 5, 6, 3, 1, and 4. The last is about 40 times weaker than the strongest line and is possibly a strain-allowed line.

For $\vec{E} \parallel \langle 111 \rangle$ (Fig. 6) the same ZFS's occur as found in the $\langle 100 \rangle$ data, and the lines can be separated into several groups having the same slope. The highest-slope lines (5 and 6) originate at 65 and 92 GHz with the former²⁷ being very well defined between 80 and 140 GHz. The next-highest-slope lines originate at 60–65 (line 2) and 140 GHz (line 3) and have slopes very nearly half that of line 5. A second 140-GHz line (line 1) has a low slope and varies nonlinearly with E up to 80 kV/cm. It may eventually become parallel to line 2 but possibly approaches a still lower slope. Weak line 9, originating near 50 GHz, also suggests a lower slope.

Finally, the 160-GHz line (line 4) remains in the quadratic region. The four data points near 50 kV/cm for frequencies from 196 to 215 GHz suggest a high-slope line, but it is not certain whether these points are primarily an extension of line 4 or line 5.

The difficulty in interpreting the spectrum at these frequencies arises because line 5 is considerably weaker than lines 1 and 3 and cannot be resolved over the range 145–182 GHz (see Fig. 6). The strong lines in order of decreasing strength are: 3, 1, 4, 5, 2, and 6, with 4 and 5 comparable.

The data for $\vec{E} \parallel \langle 110 \rangle$ are shown over a restricted frequency range (< 150 GHz) in Fig. 7. Within this range, the same ZFS's are observed, but in this case we can distinguish four different slopes. The highest-slope line (line 3) emerges from 65 GHz. Weak lines 2 and 11 have similar slopes. Two main lines, 4 and 5, have approximately half this slope, but are clearly diverging. Several weak lines, 6, 7, and 9, originating near 60 and 90 GHz, appear to have slopes similar to lines 4 and 5. A very weak line 10, appears to have an even lower slope, while lines 1 and 8, still in the nonlinear regime, appear to be approaching the lowest slope of any of the observed lines. The strong lines for this orientation in order of intensity are: 1, 4, 3, and 5.

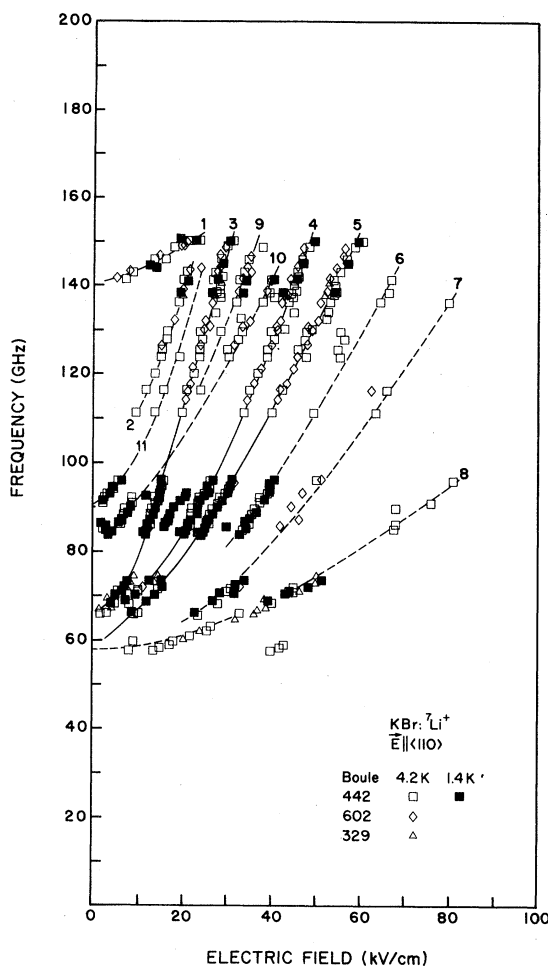


FIG. 7. Plot of the line position as a function of electric field with $\vec{E} \parallel \langle 110 \rangle$ for samples taken from several different KBr boules doped with ${}^7\text{Li}^+$. Open symbols are for $T = 4.2$ K and solid symbols are for $T \approx 1.3$ K.

B. Presentation of the ${}^6\text{Li}^+$ data

The majority of our data for ${}^6\text{Li}^+$ was taken using samples from boule 1143 and a Cornell boule, labeled as "C." The ${}^6\text{Li}^+$ spectra are greatly shifted from those for ${}^7\text{Li}^+$ as seen in Fig. 8 for two traces taken with $\vec{E} \parallel \langle 100 \rangle$ and $\nu \approx 200$ GHz. The ${}^6\text{Li}^+$ has a strong line at low- E field (22 kV/cm) (with a ZFS near 190 GHz) and a second strong line at 71 kV/cm. The ${}^7\text{Li}^+$ data on the other hand has no strong line at low field and has its strongest lines at 44 and 63 kV/cm. Clearly the spectra are quite different. The ${}^7\text{Li}^+$ data occasionally have very weak lines which correspond

quite well to the main ${}^6\text{Li}^+$ line as seen near 22 kV/cm for line *A* (Fig. 8). This, in fact, is *expected*, since naturally occurring Li^+ is used as the ${}^7\text{Li}^+$ dopant and includes roughly 7 at. % ${}^6\text{Li}^+$.

Line *B*, a relatively weak line in this trace may not belong to the ${}^6\text{Li}^+$ spectrum. Although it was observed in each boule measured, its intensity varied relative to the other lines. Since it is almost on top of the two strongest lines of the ${}^7\text{Li}^+$, it is possible that part of the intensity of line *B* arises from a low concentration of ${}^7\text{Li}^+$ in the host crystal. Alternatively, it might arise from some other as yet unidentified center, the concentration of which would likely vary from crystal to crystal, leading to a change in relative intensity. (This line is number 8 in the $\langle 100 \rangle$ data of Fig. 9.) The relative intensity of *all* other lines is consistent from boule to boule.

In Figs. 9 and 10 we present the composite data for dc and microwave fields parallel to $\langle 100 \rangle$ and $\langle 111 \rangle$, respectively. Open data points correspond to 4.2 K while filled symbols are 1.3–1.4 K. The $\langle 100 \rangle$ data show four strong lines and several weaker lines which can be grouped into high or low slopes. Lines with a high slope are: line (3), originating at 90 GHz; line 4, still in the nonlinear regime; two weaker lines emerging at 102 GHz (line 7); and line 6. The best-defined low-slope line (line 2) originates near 125 GHz, and in the high-field regime has a slope approximately half that of line 3. A second low-slope line (line 1) emerges from the 90-GHz splitting, and varies nonlinearly with E up to 80 kV/cm. Finally, a very weak line (line 5) at low frequencies is probably a low-slope line. The strong lines, in order of decreasing signal strengths, are: 2, 4, 1, and 3.

Four strong lines again appear in the $\langle 111 \rangle$ data (Fig. 10). Three lines, 2, 3, and 5, appear to have the same slope asymptotically, as well as several of the weaker lines, 6, 7, 8, and 9. A single line (1) with a splitting between 70 and 80 GHz has a much lower slope. The lines in order of decreasing intensities are: 5, 1, 3, and 2, with the latter two having comparable strengths.²⁸ (Line 4, a relatively strong line for this orientation, corresponds to the questionable line *B* above.)

C. Temperature dependence

In Fig. 3 we show two traces for boule 442 at temperatures of 4.2 and 1.4 K. The measurement frequencies are approximately 90 and 92 GHz, respectively. These traces are essentially identical

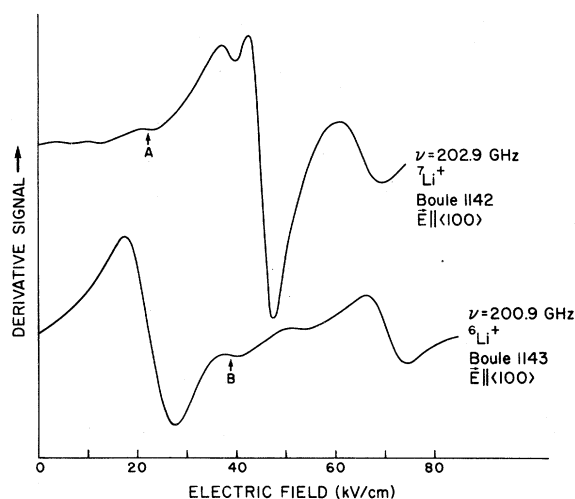


FIG. 8. Comparison of the spectra for ${}^6\text{Li}^+$ and ${}^7\text{Li}^+$ for a frequency of 200 GHz. Line *A* in the ${}^7\text{Li}^+$ trace is a weak line from naturally occurring ${}^6\text{Li}^+$. Line *B* in the ${}^6\text{Li}^+$ spectrum varies somewhat in relative intensity.

for *all* lines in the spectrum except the first dip at low- E fields. This dip is the beginning of a line with a ZFS near 92–95 GHz and its position is very sensitive to frequency and linewidth. In Fig. 11 we show another example of the weak temperature dependence at a frequency of 133.5 GHz. Some of the weaker lines appear to be somewhat stronger at 1.4 K than at 4.2 K, but by a factor of 2 at most. It is not clear whether they are in fact stronger at 1.4 K, or whether they only appear to be as a result of the disappearance of other weak lines. The first dip also appears to be a factor of 2 weaker at 1.4 K. However, this dip is just the onset of a very strong line which emerges about 141 GHz; consequently it is very sensitive to small changes in frequency and also in tuning of the spectrometer. The difference in these dips is not significant and does not show up at higher frequencies above 141 GHz. Clearly, then, a large temperature dependence of the well-defined lines is *not* observed. This result is typical for all our data for both ${}^7\text{Li}^+$ and ${}^6\text{Li}^+$ and is somewhat surprising in view of the clear temperature dependence observed in studies of $\text{KI}:\text{OH}^-$ (Ref. 15) and $\text{KCl}:\text{CN}^-$ (Ref. 29).

D. Concentration dependence

Our first attempts to measure the concentration dependence of the signal intensity used only melt-doped samples. Boules 442, 493, and 475 were

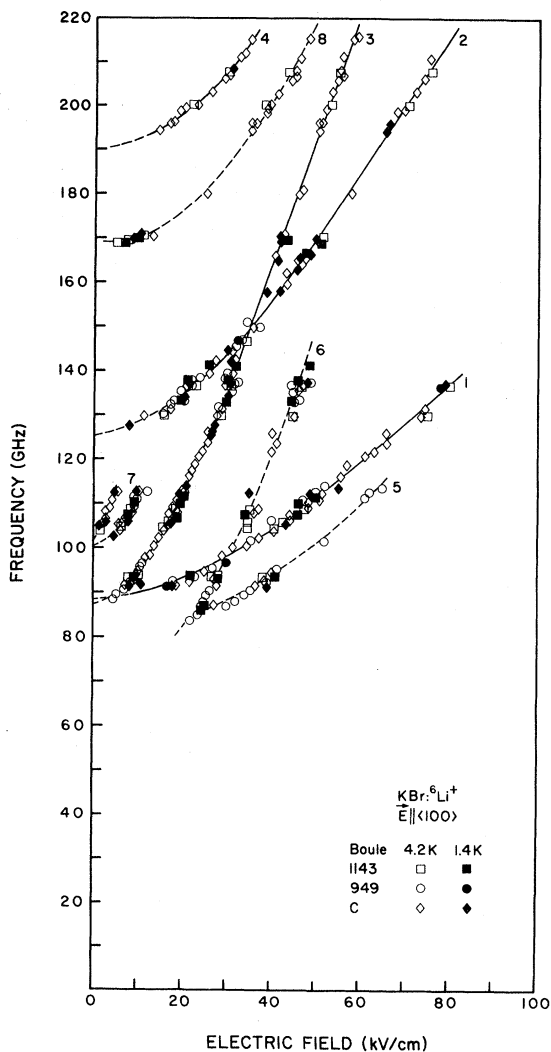


FIG. 9. Plot of the line position vs electric field with $\vec{E} \parallel \langle 100 \rangle$ for $\text{KBr}:\text{Li}^+$ samples from three boules. Open symbols are for $T=4.2$ K while filled symbols are for $T \approx 1.3$ K.

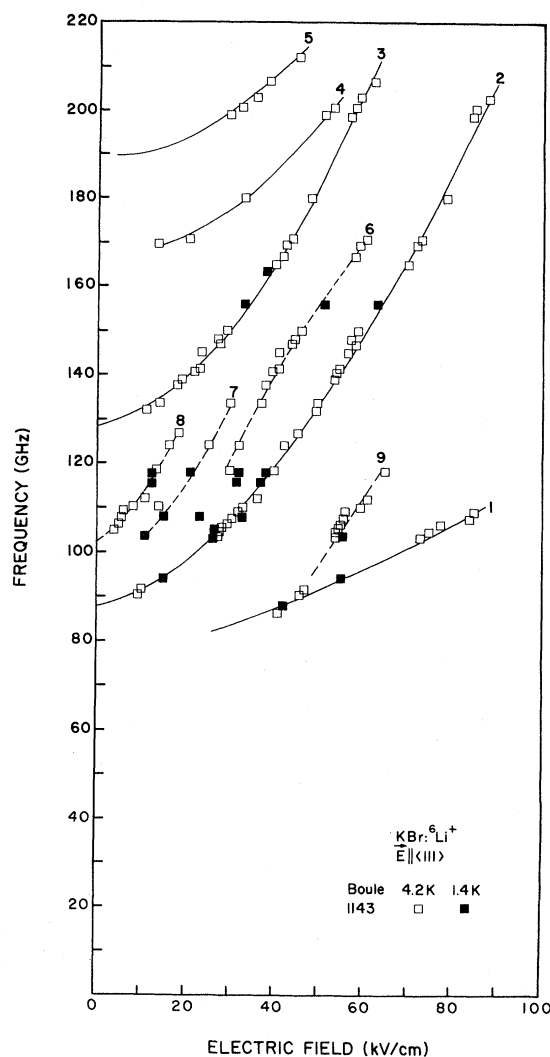


FIG. 10. Plot of the line position vs electric field with $\vec{E} \parallel \langle 111 \rangle$ for $\text{KBr}:\text{Li}^+$ samples from boules 1143. Open symbols are for $T=4.2$ K while filled symbols are for $T \approx 1.3$ K.

doped with Li^+ at concentrations which varied by a factor of 100. Unfortunately no signals were observed in boules 493 and 475 in the preliminary experiments. Further studies at high concentrations (boules 442, 329, and 602) showed that the observed intensity did not vary systematically from boule to boule with the added Li^+ concentration. We suspected that the *starting material* was important (see 6 and 7 below) and decided to dope pure KBr using a diffusion process.

After initial attempts produced strong PER signals in diffusion-doped crystals, we ran a series of experiments to measure the concentration dependence of the line intensity in the *same* host materi-

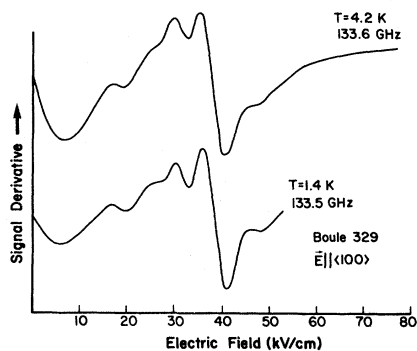


FIG. 11. Spectra for $\text{KBr}:\text{Li}^+$ at 4.2 and 1.3 K for $\nu=133.5$ GHz. Note that the relative intensities do not change with temperature. Sample was made from boules 329.

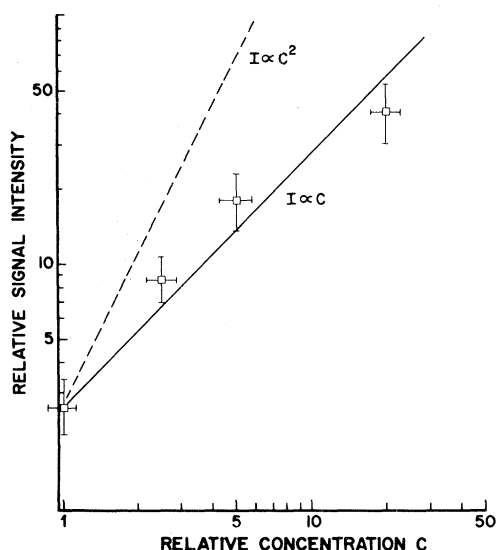


FIG. 12. Plot of the relative signal intensity as a function of relative concentration for diffusion-doped samples prepared using the *same* starting material. Signal intensity increases linearly with concentration at these low concentrations.

al (see Sec. IIB for details). We prepared four samples whose concentrations varied by a factor of 20. The concentration of the highest-doped sample was measured at ≤ 40 ppm (Li^+ ions per K^+). The relative signal intensity is plotted as a function of relative concentration in Fig. 12. The results clearly fit a *linear* dependence and do *not* follow a quadratic dependence (indicated for reference by a dotted line). The highest point, however, suggests that the curve may be turning over, possibly indicating the onset of saturation as observed by Thörmer and Lüty³⁰ in $\text{RbCl}:\text{Li}^+$.

E. Quenching

Samples from boule 602 show the same spectra as samples from all other boules for frequencies up to 150 GHz and for all field orientations with one exception: a very strong (60–65)-GHz low-slope line which in our $\langle 100 \rangle$ data is slightly shifted from line 1. The relative intensity of line 1 to line 3 is 20:1 (Fig. 13, trace *a*), whereas for all other boules, the intensity ratio of line 1 to 3 is 1:4, trace *b* [for data taken in the (84–96)-GHz range]. In contrast, at higher frequencies, the relative intensity of lines 3 and 5 is the same as for samples from other boules suggesting that only line 1 is anomalous. Diffusion-doped samples, using the

pure end of boule 602, however, show the *usual* intensity ratio.

Because of the unusual behavior of this boule, we tried various heat treatments. The spectra of annealed samples are essentially unchanged, except for a slight narrowing of the resonances. On the other hand, with quenched samples we obtain a striking result: *After* quenching, the intensity ratio of lines 1 and 3 is now 1:4, the *same* as the ratio obtained for the other boules. The anomalous line has essentially disappeared, as seen in Fig. 13, traces *c* and *d*, where samples from boules 602 and 442 are compared after quenching.

We also measured the relative intensity of the 141-GHz high-slope line (line 5) of the 602 sample before and after quenching using the $\text{KCl}:\text{Li}^+$ sample for calibration. We found another striking result: Quenching the 602 sample *enhanced* the intensity of this line by a factor of 10–20.

We then tried quenching samples from each of our other boules. In the case of 442, the sample showed no significant increase in intensity, but the lines broadened (see Fig. 13) probably as a result of increased internal strains. In a sample from boule 493, which had previously shown *no* signal, howev-

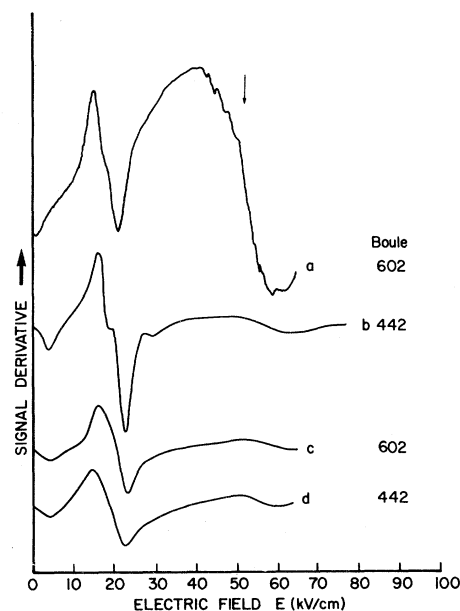


FIG. 13. Comparison of spectra obtained for boules 442 and 602 at 4.2 K before and after quenching. Very strong line (indicated by the arrow for trace *a*) in the original 602 spectrum is missing in the quenched spectra (trace *c*). Signal from boule 442 is considerably broadened after quenching (trace *d*).

er, a signal *appeared*. Though it was broad and weak, it seemed quite consistent with the data obtained using other boules. Similar enhancements, up to a factor of 1000, were found in many other samples, and in *no* case did the quenching procedure diminish the PER signal. Moreover, quenching of samples from other boules showed *no* change in relative intensities of the strong lines.

F. OH⁻ and other impurities

The results of quenching indicate that the observed signal is sample-preparation dependent, and may, for example, depend on small amounts of trace impurities. One such possibility is OH⁻, suggested by Lüty's³¹ result that the OH⁻ concentration is enhanced in lithium-doped samples.

We undertook several experiments involving OH⁻ in KBr:Li⁺ materials. In one series, we prepared identical samples of pure KBr material. Into one sample we diffused LiOH, and into the other we diffused LiBr. We found that the LiBr-doped samples always gave PER signals, while no signals were detected in the LiOH-doped samples. In a second series of tests, we started with KBr:Li⁺ samples which gave a strong PER signal. We then diffused KOH into these samples; invariably, the PER signal previously present was partially suppressed, or entirely absent. In the third series of tests we diffused LiBr into samples from a boule of KBr doped with KOH in the melt. No signal was observed after a 1-day diffusion but a weak signal, resembling our usual spectra finally emerged after a much longer diffusion (5–6 days) with additional amounts of LiBr dopant.

These tests suggest that OH⁻ acts to *suppress* the PER signal in lithium-doped KBr.³² We therefore ordered a boule (1014) of pure KBr and a quantity of LiBr, both especially treated to exclude the presence of OH⁻. However, PER measurements on diffusion-doped samples from these materials initially showed *no* observable lines (Fig. 14, traces *a* and *b*) indicating that, although OH⁻ was probably not present, some *other* suppressive mechanism must be active in this boule. Again, upon quenching this sample, a strong signal appeared with an increase of signal intensity of more than 100 (Fig. 14, trace *c*). Here *B* is the KCl:Li⁺ calibration signal and *A* is the expected position of the KBr:Li⁺ signal.

We also attempted to diffuse Na⁺, F⁻, Cl, and I⁻ into pure-KBr samples with no significant effects. We annealed melt-doped samples from boule

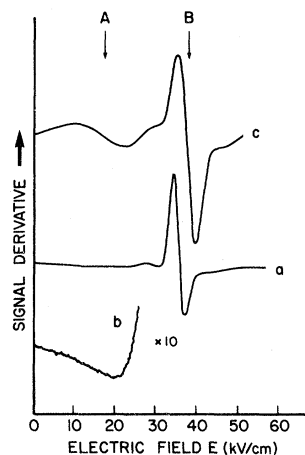


FIG. 14. Change in intensity of the main KBr:⁷Li⁺ signal after quenching a diffusion-doped sample from boule 1014. *A* indicates the expected position of the KBr:⁷Li⁺ signal while *B* gives the position of the KCl:⁷Li⁺ reference signal. No KBr:⁷Li⁺ signal is observed before quenching (trace *a*) even with a 10-times increase in gain (trace *b*). A strong signal is, however, observed after quenching (trace *c*).

442 in hydrogen and oxygen atmospheres and observed little change in the PER signal. Using uv, we also irradiated a slice of boule 329 (which had been melt doped with *U* centers) to form *F* centers, but no change in the PER data was observed.

V. DATA ANALYSIS

A. Preliminary analysis

1. Slopes and dipole moments

In Table II we have estimated the slopes of some of the main lines for each isotope and field orientation. If we had reached the high-field linear regime, those slopes would represent the full dipole moment of the system. However for KBr:Li⁺, even the lines with the best-defined slopes are still partially in the nonlinear regime and the measured slope will be a little lower (typically 10%) than the high-field value. Many lines exhibit curvature over the entire range of observation and hence only a lower limit to the slope can be estimated.

For $\vec{E} || \langle 100 \rangle$ most lines fall into two groups, with the highest-slope lines being best defined. Within the range of our data, the ratio *R* of the slopes for the two groups appears to be approaching 2:1; i.e., for ⁷Li⁺ $R \approx 2.6/1.2 = 2.2$ and for

TABLE II. Slopes of best-defined lines [slopes in GHz/(kV/cm)].

${}^7\text{Li}^+$			${}^6\text{Li}^+$		
Line	Slope	Comment	Line	Slope	Comment
$\vec{E} \langle 100 \rangle$					
3	2.6	Well defined	3	2.8	Well defined
4	2.5	Fairly well defined	4	>2	Still in nonlinear range
5	≥ 2.5	Nonlinear range	8	>2	May not be ${}^6\text{Li}^+$ line
1	≥ 1.2	Still in nonlinear range	2	1.5	May still be in nonlinear range
8	>4.0	Weak line, quite well defined only from 100–140 GHz			
$\vec{E} \langle 111 \rangle$					
5	3.1	Well defined	2	>2.1	Nonlinear range
2	>2.2	Still nonlinear	3	>2.1	Nonlinear range
1	>0.9	Still close to zero-field splitting	1	>0.6	Still close to zero-field splitting
$\vec{E} \langle 110 \rangle$					
3	3.5	Quite well defined			
4	≥ 2.7	Still nonlinear			
5	≥ 2.2	Still nonlinear			
1	>1.5	Still nonlinear			
8	>0.8	Close to zero-field splitting			

${}^6\text{Li}^+$ $R \approx 2.8/1.45 = 1.9$. A 2:1 ratio is expected for $\langle 100 \rangle$ or $\langle 110 \rangle$ paraelectric systems. (A $\langle 111 \rangle$ model admits only a single slope for $\vec{E}||\langle 100 \rangle$ data.) In addition there is a weaker but quite well-defined line, over the (100–140)-GHz range with a much higher slope—line 8, Fig. 5 (it may well be a factor of 2 higher). This line is not consistent with any of the *standard*¹⁵ models and will be ignored in attempts to fit the data to such models.

For $\vec{E}||\langle 111 \rangle$ the best-defined ${}^7\text{Li}^+$ slope (3.1 GHz/bar) is a factor of 1.2 higher than the strong ${}^7\text{Li}^+$ high slope for $\vec{E}||\langle 100 \rangle$. This is consistent with the value 1.15 expected for a $\langle 110 \rangle$ model (but not for a $\langle 100 \rangle$ model). Although the low-

slope lines are still well within the nonlinear regime, they are quite consistent with the slopes observed in theoretical calculations for a $\langle 110 \rangle$ model with a large ZFS [large in the sense that the largest ZFS's are within a factor of 2 of the highest microwave frequency (217 GHz) available with our spectrometer]. The ${}^6\text{Li}^+$ data also appear consistent only with a $\langle 110 \rangle$ model, although the slopes are less well defined over the range of our measurements.

Finally for $\vec{E}||\langle 110 \rangle$ several slopes are observed for ${}^7\text{Li}^+$. Using the high slope for $\vec{E}||\langle 100 \rangle$ and a $\langle 110 \rangle$ model one expects four possible slopes: 3.6, 2.7, 1.8, and 0.9. These are quite consistent with the experimental results.

TABLE III. Zero-field splittings (GHz).

⁷ Li ⁺		⁶ Li ⁺	
Splitting	Comments	Splitting	Comments
161±3	Well defined	195±5	Well defined
141±3	Well defined	127±3	Well defined
95±3	Well defined	103±2	Well defined
65±2	Well defined	88±2	Well defined
130–150	Strong line 2 (Fig. 5)	167±3	Questionable line 8 (Fig. 9)
59–65	Line 1 (Fig. 5)	70–80	Line 1 (Fig. 10)
48–52	Weak line 9 (Fig. 6)		
50–65	Several lines (Fig. 7)		

In principle, one expects to extract a unique dipole moment from the data, whose magnitude depends both on the particular model and on a detailed fit of the model to our high-field data. The observed slopes provide an initial estimate of the dipole moment, which will be used as a starting value in a fit of the data to a $\langle 110 \rangle$ model.

2. Zero-field splittings

In the above measurements, the ZFS's have been obtained by extrapolating the frequency versus the electric field plots back to zero electric field assuming that the E -field dependence is quadratic in this regime. However, no corrections for broadening interactions have been included. If the main broadening is via random electric fields then the electric field linewidth will not change very much with E field and the extrapolated ZFS will be higher than the actual value (i.e., the value with no broadening) by almost a frequency linewidth.²⁶ On the other hand if the frequency linewidth is constant (and symmetric), then the electric field linewidth will be large for low E , and will decrease with increasing E field. The line shape will be dis-

torted at low- E field, but the "zero crossing" of the derivative signal will give the correct line position (i.e., the position with no broadening) and no effective shift of the extrapolated ZFS occurs. Since in our data the lines clearly narrowed with increasing E field, the E -field broadening is not dominant and we have not made any corrections for it. At most, we estimate that this correction might lower the observed splittings by 2–3 GHz. The zero-field splittings are tabulated in Table III.

3. Similarities and differences between the ⁷Li⁺ and ⁶Li⁺ data

Overall, the spectra for both ⁶Li⁺ and ⁷Li⁺ are quite similar, the main difference being the shift in the zero-field splittings from the range 52–160 GHz for ⁷Li⁺ to 75–190 GHz for ⁶Li⁺. Generally the lines appear to move to higher frequency when ⁶Li⁺ replaces ⁷Li⁺ although at least one line may move in the opposite direction.

The slopes for both isotopes are quite similar, indicating that the dipole moments are the same within 8–10%. Since, for the best-defined slopes

TABLE IV. Isotope shifts.

⁷ Li ⁺			⁶ Li ⁺			% shift
Line	Electric field orientation	Splitting	Line	Electric field orientation	Splitting	
1	$\langle 100 \rangle$	60	1	$\langle 100 \rangle$	89	48%
3	$\langle 100 \rangle$	65	3	$\langle 100 \rangle$	89	35%
2	$\langle 100 \rangle$	~140	2	$\langle 100 \rangle$	127	-9%
5	$\langle 100 \rangle$	140	5	$\langle 100 \rangle$	190	36%
9	$\langle 111 \rangle$	~50	1	$\langle 111 \rangle$	~75	50%
3	$\langle 111 \rangle$	140	3	$\langle 111 \rangle$	127	-9%

in the $\vec{E}||\langle 100 \rangle$ data, the ${}^6\text{Li}^+$ slope is consistently larger than the ${}^7\text{Li}^+$ slope by 8–10%, there may well be some small difference in the off-center position for the two isotopes. However, we will ignore this aspect in the present analysis.

We now propose a tentative identification of corresponding lines in the ${}^6\text{Li}^+$ and ${}^7\text{Li}^+$ data. The criteria for such associations are: similar slopes in the high-field regime, similar curvature in the low-field regime, and similar relative intensities. For example, in the $\langle 100 \rangle$ data one pair of lines is easily identified in each spectra; the two main lines for ${}^7\text{Li}^+$ emerging from 60–65 GHz (lines 1 and 3, Fig. 5) correspond to the two lines at 89 GHz in the ${}^6\text{Li}^+$ data (lines 1 and 3, Fig. 9). The identifications are given in Table IV. The three following points, however, deserve further comment:

(1) One of these identifications implies a *negative* isotope shift. However, such a result is not unexpected since the splittings can be the algebraic difference of two (or more) tunneling parameters.

(2) Although we have identified strong line 1 of the ${}^6\text{Li}^+$ $\langle 111 \rangle$ data with line 9 of the corresponding ${}^7\text{Li}^+$ data, the latter line is very much weaker. This may be due to an accidental cancellation of terms in the transition element.

(3) It is quite possible, particularly for ${}^6\text{Li}^+$, that allowed PER transitions exist with zero-field splittings above the range of our spectrometer. This could change the identification of corresponding lines for the higher zero-field splittings.

4. Temperature dependence

In measurements at 1.4 and 4.2 K, we found the surprising result that, unlike many other paraelectric species,^{24,28} the KBr:Li^+ spectra show *no* significant temperature dependence. This implies that the transitions arise either from the ground state, or from some state within 30–40 GHz of the ground state. Since measurements down to 42 GHz provide no evidence for smaller splittings, it is quite likely that most of the observed splittings do originate from the ground state of the system.

5. Single center or several distinct centers?

Before attempting to fit the data to any specific model, it is important to determine whether the ob-

served spectra arise from a *single* (possibly complex) center or whether it is a *composite* spectra resulting from several distinct centers. The most striking argument comes from the observation of the same spectra in *seven* different boules grown at different times and from different source materials over a five-year period. The strong lines in both the ${}^7\text{Li}^+$ and ${}^6\text{Li}^+$ data are consistent in position and in relative intensity, for both *melt*-doped and *diffusion*-doped samples for all orientations of electric field (see Sec. IV). In addition a search for PER signals from likely *contaminants* of KBr (F^- , Cl^- , Na^+ , OH^- , H^+ , O_2) gave negative results.

It is, of course, true that other centers exist, evidenced by the anomalous line(s) found in boule 602. However, the PER of this anomalous center could easily be distinguished from the rest of the spectra using intensity-ratio measurements and by quenching. *None* of the other strong lines in our data, however, showed *any* significant shift in position or change in relative intensity from heat treatments.³³

These results strongly suggest that the observed signal arises from a *single* center. In order for the spectra to be a composite of the spectra from several centers, the concentration levels would always have to be proportional to one another, independent of the starting material, of the added dopant level, and of heat treatments.

6. Evidence that the signal arises only from lithium centers

The strongest evidence that the signals arise from Li^+ comes from two observations: the large isotope shift of the ZFS and the linear concentration dependence. When ${}^6\text{Li}^+$ replaces ${}^7\text{Li}^+$, the *entire* spectrum shifts although the high-field slopes obtained from the strong lines remain essentially unchanged. Different ZFS are shifted different amounts, but for many lines this shift is in the 35–50% range. Such a large isotope shift not only indicates that the signals arise from Li^+ but also that the Li^+ ion must undergo a *tunneling* motion. Transition from the ground state to an excited state in an harmonic well or square well would give an 8.5% or 17% shift, respectively, far less than that observed. Because of the exponential mass dependence, however, tunneling easily produces a large isotope shift. Thus the signals we observe most likely arise from a single lithium center in which the lithium ion is tunneling.

B. Attempts to fit the data to specific models

1. Single-multiplet tunneling models

Here we attempt to fit the data to the $\langle 110 \rangle$ tunneling model¹⁵ discussed previously (Sec. III) assuming the tunneling species is a single off-center Li⁺ ion. We considered and rejected the $\langle 100 \rangle$ and $\langle 111 \rangle$ models earlier,¹⁴ based on data taken up to 150 GHz. Whereas the standard $\langle 100 \rangle$ model has only one slope for $\vec{E} \parallel \langle 111 \rangle$, and the $\langle 111 \rangle$ only one slope for $\vec{E} \parallel \langle 100 \rangle$, our data show two slopes for *both* these orientations. The additional ZFS found above 150 GHz reinforce this conclusion; there are far too many *independent* splittings for either the $\langle 100 \rangle$ or $\langle 111 \rangle$ model.¹⁸

For the strong lines, the number of slopes and the ratio of slopes between various field orientations are all essentially consistent with a $\langle 110 \rangle$ model. [Some of the weaker lines, such as line 8 observed in the ${}^7\text{Li}^+ \vec{E} \parallel \langle 100 \rangle$ data, are not consistent and have too large (or too low) a slope.] Therefore, we carried out a thorough analysis of the strong lines of the ${}^7\text{Li}^+$ data.

The initial conclusion is straightforward: If all the observed ZFS's (52, 60, 65, 95, 141, 130–150, and 160 GHz) are distinct, there is no way that the simple $\langle 110 \rangle$ model can account for them. In the $\langle 110 \rangle$ model, there are at most four independent splittings. In our data, however, only one, or at most two, ZFS's can be accounted for by a sum rule. Thus to stay within the $\langle 110 \rangle$ model, we must assume that several of the observed lines originate from the same ZFS. For example, the ZFS near 60 GHz might all be the same, as might those at 141 and 130–150 GHz. However, an important result of the previous paper¹⁸ is that no two *allowed* lines in the $\langle 100 \rangle$ data of the $\langle 110 \rangle$ model can have the same zero-field splitting. Hence, some must be either strain-allowed or internal electric-field-allowed transitions. We therefore assume that some of the observed transitions are forbidden, and in the rest of the analysis, the weaker 52- and 95-GHz lines are ignored. Furthermore, in most cases we also let one or more of the remaining lines be strain allowed.

In our initial fit, we ignored temperature dependencies, made no assumption about the relative sizes of the tunneling parameters, or even their *signs*.³⁴ Following the method presented in the previous paper,¹⁸ we searched through each of the possible 24 diagrams and found that only the following could plausibly fit the data: diagrams 1, 2, 13, 15, 23, and 24. A stringent condition in reduc-

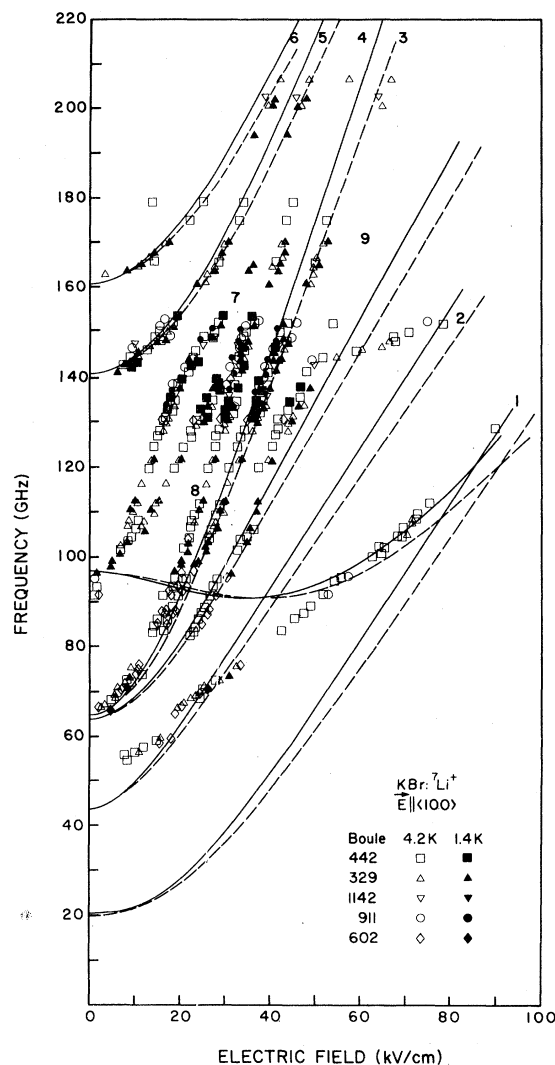


FIG. 15. One of the best attempts to fit the ${}^7\text{Li}^+$ data to a $\langle 110 \rangle$ tunneling model for $\vec{E} \parallel \langle 100 \rangle$. Some lines can be fit extremely well while others are not fit at all. Parameters $\eta = -13.88$, $\mu = 3.25$, $\nu = 10.38$, and $\sigma = -53$ GHz; $p = 0.95 e \text{ \AA}$ —solid line, and $p = 0.89 e \text{ \AA}$ —dashed line.

ing the number of possible diagrams was the requirement in the $\langle 111 \rangle$ data of a high-slope line with a ZFS of 65 GHz (line 5). For each of these diagrams, we found several possible ways to identify experimental splittings with allowed transitions. Once each such assignment was made, the values of the corresponding tunneling parameters were uniquely determined. From each such set of parameters, we numerically generated the theoretical positions of the resonance lines as a function of electric field and compared it with the data in Figs. 5 and 6. Of the fifteen best such possibilities, none gave a good fit for *all* the main lines in either

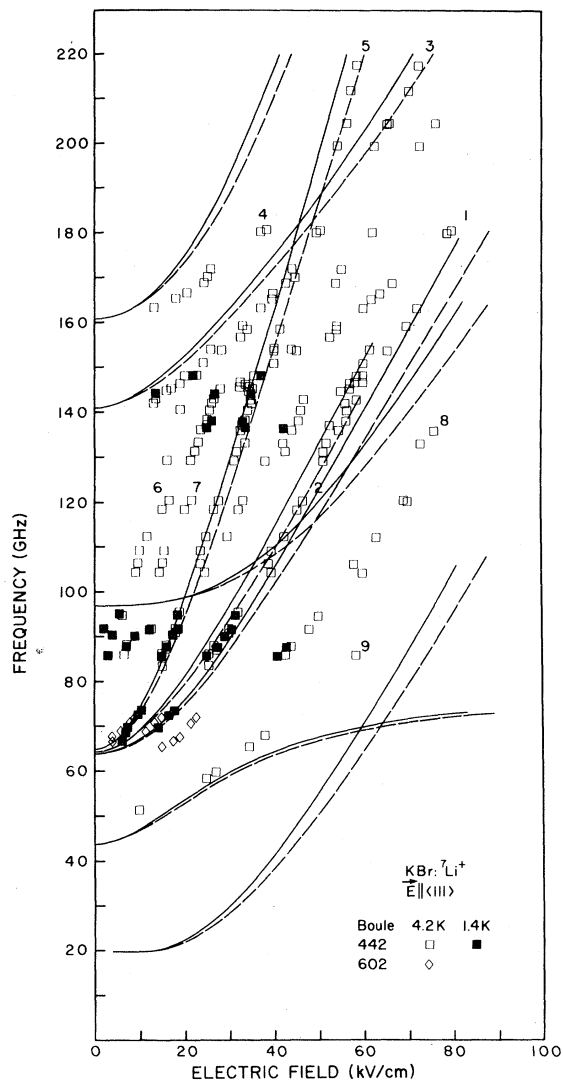


FIG. 16. Fit to the data for $\vec{E}||\langle 111 \rangle$ using the same parameters as in Fig. 15.

$\langle 100 \rangle$ or $\langle 111 \rangle$ data. However, we could often fit two or three main lines in both orientations well. One example is given in Figs. 15 and 16 for two field orientations using the following tunneling parameters: $\eta = -13.88$, $\mu = 3.25$, $\nu = 10.38$, and $\sigma = -53$ GHz. To obtain the very best fit for the high-slope lines, we apparently also need a slightly different dipole moment (uncorrected for local field) than that required to give the best fit to the low-slope lines as indicated by the solid and dashed lines ($p = 0.95$ and $0.89 e \text{ \AA}$, respectively). To show that a fit of this quality is not entirely unique, we show a second fit for the $\langle 100 \rangle$ data in Fig. 17 obtained from diagram 2, with the following tunneling parameters: $\eta = -30.83$, $\mu = 32.67$, $\nu = -6.88$, and $\sigma = -13.83$ GHz. Surprisingly,

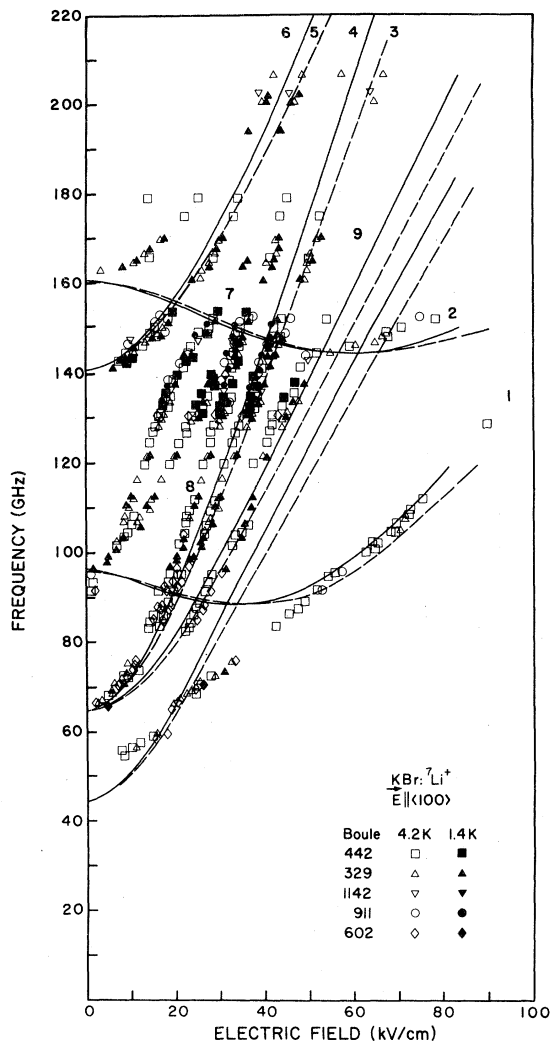


FIG. 17. Second "best" attempt to fit the ${}^7\text{Li}^+\vec{E}||\langle 100 \rangle$ data to a $\langle 110 \rangle$ model with $\eta = -30.83$, $\mu = +32.67$, $\nu = -6.88$, and $\sigma = -13.83$ GHz. Note that these tunneling parameters are very different from those used for Fig. 15. The dipole moments are the same as those used in Figs. 15 and 16.

these two sets of tunneling parameters are quite different, and in both cases they require some *positive*³⁴ values. The lack of a good fit for all the strong lines clearly indicates that the 12-state $\langle 110 \rangle$ model does not have sufficient complexity to explain the KBr:Li⁺ data.

2. Tunneling models with several multiplets

Following the ideas developed for the KI:OH⁻ system,²⁵ one might suggest that two or more multiplets should be considered to describe KBr:Li⁺. However, unlike the OH⁻ system, there appears to be no simple reason why a *low-lying* second multiplet should exist. In the OH⁻ system, the two

multiplets were attributed to the possibility that the OH⁻ ion may be off center in two different ways: with the intrinsic molecular dipole parallel or antiparallel to the off-center dipole. (It could be even more complicated.) However, for the off-center KBr:Li⁺ case, the impurity does not carry an intrinsic dipole moment. Of course, an additional multiplet of tunneling energy levels should exist centered about the first excited state at an energy E_1 above the ground state. However, the energy E_1 is expected to be much larger than any of the splittings we have observed, based²⁵ on a square-well potential model of width less than 1 Å. Consequently, we have no simple reason to expect that a second low-lying multiplet should exist for Li⁺ and we do not pursue such a model further at this time.

3. Complex lithium centers

Because of the difficulties fitting the data to a single model, and the fact that only a small fraction of the added Li⁺ ions is probably active, we have considered the possibility that the observed signal arises from a Li⁺ complex including Li⁺ pairs. Five such models were outlined briefly in Sec. III.

The main experimental evidence *against any* complex Li⁺ center is found in the quenching experiments. An increase in integrated signal intensity is obtained for quenched samples; annealed samples, on the other hand, show no significant change in the signal (a slight narrowing). At the high temperature, most of the Li⁺ ions should move rapidly within the crystal rather than be trapped at vacancies or by other impurities. Consequently, this technique should produce more *individual* Li⁺ ions, and we have interpreted these results as strong evidence against a Li⁺ complex.

One type of defect whose concentration increases with quenching is the vacancy, and one might argue that the observed signal is a Li⁺-vacancy complex. However, not *all* boules showed a strong signal intensity increase upon quenching. In particular, boule 442 (a high-concentration boule) showed *no* increase in integrated signal intensity upon quenching, but did show considerable broadening of the resonance lines, indicating that the internal random strain (and hence the number of vacancies) had increased.

In addition to this negative evidence for a Li⁺ complex, we also compared our data with the complex models (Appendix A) and showed that *none* of

them provide a good explanation for our data. The arguments against these models are:

- (a) The Li⁺:X⁻ and Li⁺:Y⁺ models do not have enough ZFS's to explain the six observed ZFS's.
- (b) The models for Li⁺:Y⁺ (including Li⁺ pairs) give only *one* slope in a plot of resonance frequency as a function of electric field for $\vec{E} \parallel \langle 100 \rangle$, in contrast to the data.
- (c) The $\langle 100 \rangle$:X⁻ model predicts backward lines

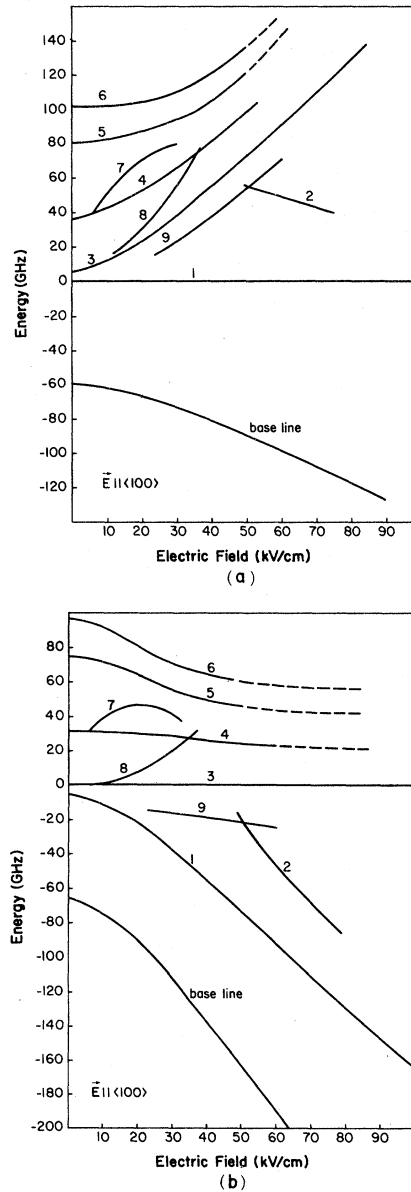


FIG. 18. Possible energy-level diagrams for ${}^7\text{Li}^+$ with $\vec{E} \parallel \langle 100 \rangle$. In (a) we assume line 1, Fig. 5, is a transition from the ground state to a field-independent state, while in (b) line 3 is assumed to be such a transition.

for both $\langle 100 \rangle$ and $\langle 111 \rangle$ field orientations and only one slope for $\vec{E} \parallel \langle 111 \rangle$. Both are in disagreement with the data.

(d) The $\langle 111 \rangle : X^-$ model predicts some backwards lines and only one slope for $\vec{E} \parallel \langle 100 \rangle$ again in disagreement with the experimental results.

(e) The $\langle 110 \rangle : X^-$ does provide for a large number of possible ZFS's. However, it suggests backwards lines for both the $\langle 100 \rangle$ and $\langle 111 \rangle$ field orientations in contrast to the experimental results.

C. A possible energy-level diagram

We can obtain a partial energy-level diagram if we assume that all observed transitions arise from the ground state. This is consistent with the observed lack of temperature dependence of the spectra. Since we also expect the lowest energy level to be decreasing in energy with field (while other levels are constant or increasing with field), we must decide which lines represent transitions from the ground-state to the field-independent levels. For $\vec{E} \parallel \langle 100 \rangle$ two possibilities exist: We can choose line 1, Fig. 5, as the transition to a field-independent state, or we can choose lines 3, 4, and 5. The former [Fig. 18(a)] would be consistent with our attempts to fit the data to one of the standard models but would not suggest a simple explanation of the weak lines, 7 and 8, which appear to have a higher slope. The latter case makes these weak lines more symmetric as shown in Fig. 18(b), suggesting perhaps that more equivalent off-center dipole positions are possible or that more than one dipole moment is observed. Further, this figure is also suggestive that lines 7 and 2 may in fact be part of the same line.

VI. DISCUSSION OF RESULTS AND COMPARISON WITH OTHER EXPERIMENTS

A. Summary of experimental results

The experimental results and the analysis presented in the preceding two sections indicate that $\text{KBr}:\text{Li}^+$ is a very unusual paraelectric-paraelastic system. The main features that emerge from this extensive study are:

(1) The relative intensity of the various lines is the same in seven $\text{KBr}:\text{Li}^+$ boules, and in three $\text{KBr}:\text{Li}^+$ boules, indicating that the signal arises

from a single type of center.

(2) In a series of diffusion-doped samples the signal intensity varies linearly with concentration, suggesting that *single* Li^+ ions are involved.

(3) There is a large isotope shift of the ZFS (35–50%) when $^6\text{Li}^+$ replaces $^7\text{Li}^+$. This indicates that the Li^+ ion is *tunneling* in some multiwell potential.

(4) The data and analysis indicate considerable symmetry for this system. For a given set of tunneling parameters and a given dipole moment a $\langle 110 \rangle$ model provides a good fit (both slope, curvature, and ZFS) to some of the lines in *each* orientation of electric field.

(5) The curvature of the 140-GHz line ($^7\text{Li}^+$) over a fairly large frequency range as well as the large isotope shift indicates that this splitting (and likely the 160-GHz) is a *tunneling* splitting and not a (diagonal) splitting between two multiplets.

(6) Quenching the samples usually increases the signal intensity, sometimes by very large factors (10–1000). This suggests that at high temperatures, the Li^+ ion is dispersed throughout the crystal and that some isolated ions are frozen into the lattice upon quenching before they can be trapped at other sites.

(7) Several $\text{Li}^+ : X^-$ and $\text{Li}^+ : Y^+$ complex centers were also considered but clearly could *not* explain the main features of the data.

(8) Figure 18(b), obtained by assuming that all transitions arise from the ground state, is suggestive of either additional off-center positions or an additional dipole moment.

(9) Some additional impurities in KBr tend to *suppress* the observed signal. OH^- is one such impurity, but it is probably not the only one.

Consequently the number of active centers is considerably *less* than the amount of Li^+ actually in the crystal.

The suppression of the Li^+ signal either by the presence of other impurities or perhaps by clumping of the Li^+ ions is unusual but not unique in paraelectric systems. Ag^+ in RbCl also tends to clump and the signal intensity is enhanced by quenching.³⁵ We cannot make an *accurate* estimate of the number of active ions without a good model. Assuming a $\langle 110 \rangle$ model, we computed the transition matrix elements for several choices of dominant tunneling parameter and then calculated the expected theoretical intensities of the strongest lines. Using these results, and the observed signal intensities (obtained using the $\text{KCl}:\text{Li}^+$ reference sample), we conclude that we

are observing only 10^{-3} to 10^{-1} of the Li⁺ in the KBr crystal. This result alone may explain some of the earlier negative results.

B. Comparison with other results

Most of the early investigations³⁻⁶ of KBr:Li⁺ showed no evidence for paraelectric behavior. In many cases no signals were observed at all while in a few cases some signal was observed with properties unlike that of the other well-known paraelectrics. We can understand those negative results in view of the rather large tunnel splittings observed and/or the fact that only a small fraction of the added lithium ions are active. We first discuss these negative results and then briefly consider other experiments which indicate that KBr:Li⁺ is a tunneling off-center system.

Electrocaloric or paraelectric cooling experiments were first carried out on KBr:Li⁺ by Lombard and Pohl⁵ in 1965 and a few years later by Kapphan.⁶ In both experiments, no observable cooling was obtained within the experimental errors. Similarly, measurements by Harrison *et al.*⁴ in 1968 over the temperature range 0.4–1.8 K showed no dipole contributions to the specific heat within the experimental error of 5%. In both cases, these negative results can be attributed to the large tunneling splittings and the small fraction of active lithium centers. For example, in the specific-heat measurements⁴ the maximum of the dipole contribution should occur near 3 K. If we consider the case with the maximum possible lithium concentration that can be achieved (500–1000 ppm), and assume also that all of the lithium is active, then at most 40–50% of the total specific heat might be attributed to the dipoles in the 1.0–1.8 K temperature range. However, if only 10% of the lithium are active, this contribution drops to 4–5%, i.e., within the experimental uncertainty reported. Furthermore, in most cases the fraction of active centers appears to be considerably smaller than 10% in unquenched samples.

Thermal-conductivity measurements by Bauman *et al.*³ over the temperature range 0.05–100 K showed two clear resonances for KBr:Li⁺ occurring at 1 and 13 K, with the latter being the stronger resonance. For the similar case of KCl:Li⁺, the resonances occur at 0.4 and 20 K. Although the 1-K resonance was quite comparable in some regards to the KCl:Li⁺ resonance at 0.4 K and in fact also agrees with our 60-GHz resonance zero-field splitting, it was not attributed to a tunneling system based on the assumption³⁶ that all

the added lithium ions are *active*. Since PER results show only a small number of active centers, the thermal-conductivity data is, in fact, quite consistent with that of other paraelectric tunneling systems. A measure of the isotope shift for this line might well have identified it as a tunneling transition, but this, unfortunately, was not carried out.

Another extensive investigation of Li⁺-doped KBr has focused on the far-infrared-active mode at 16.3 cm^{-1} for ⁷Li⁺ which corresponds well with the higher-temperature dip of the thermal-conductivity data. Sievers and co-workers⁷⁻¹² found that this mode has a small isotope shift (10%) and essentially no electric dipole moment. Further, at high hydrostatic pressure the frequency of this mode increases monotonically.^{11,12} This is quite similar but not identical to the behavior of KCl:Li⁺ at pressures high enough that the Li⁺ ion moves on center in KCl. Sievers and co-workers assumed that this infrared mode arises from single Li⁺ centers with the Li⁺ ion on center in KBr.

It is clear that the infrared-active modes do not arise from the same centers that produce the PER spectra; otherwise a larger dipole moment would have been observed as well as several transitions separated by $3-5\text{ cm}^{-1}$, instead of a single line. The strongest PER lines have in fact been found in far-infrared measurements,^{37,28} but their intensity is at least 2 orders of magnitude smaller than the 16.3-cm^{-1} line. Such a ratio is not inconsistent with our estimate that only a small percentage of the added Li⁺ form a paraelectric center. Thus, the question that must be considered is: Which of the observed centers—the infrared-active or the paraelectric center—corresponds to isolated Li⁺? We address this question later.

Evidence in favor of a paraelectric tunneling system has been found in two experiments in addition to the PER experiments reported here. In 1975, Ohkura *et al.*³⁹ measured the spin-lattice relaxation time T_1 of $F_A(\text{Li}^+)$ centers in KBr [the $F_A(\text{Li}^+)$ center is formed by an F center adjacent to a Li⁺ ion] and observed anomalous effects. Whereas the T_1 of F centers is independent of temperature at low temperatures, $F_A(\text{Li}^+)$ centers show a strong temperature dependence, and in addition show a large isotope dependence when ⁶Li⁺ replaces ⁷Li⁺ in the crystal. Such a strong effect can be understood if the F center experiences a fluctuating field as a result of the Li⁺ tunneling from one orientation to another.

Very recently, phonon studies⁴⁰ of KBr:Li⁺ have found a number of resonances which shift with

uniaxial stress and exhibit a large isotope shift of the zero-field splittings. Several of these splittings agree well with those observed in the PER measurements even though, in general, different transitions are allowed. The phonon resonances clearly arise from the same center as that which produces the PER lines, indicating that this center is *both* paraelectric and paraelastic as are *all* other paraelectric systems. Attempts to fit the phonon data to a $\langle 110 \rangle$ model also met with limited success, confirming the conclusion based on PER data that KBr:Li^+ is too complex to be completely described by the standard tunneling models.

C. The paraelectric and infrared-active centers

Two distinct centers are observed in lithium-doped KBr—the paraelectric-paraelastic center observed in PER and phonon resonance, and the non-tunneling center observed in far-infrared measurements. Many of the PER experiments were aimed at clarifying the nature of the paraelectric center and strongly suggest that this system is an off-center isolated Li^+ ion in KBr. The quenching experiments particularly support this hypothesis and appear inconsistent with a simple Li^+ —impurity-ion complex.

Though such complexes most likely do exist in the crystal, they are *not* responsible for the PER signals. For example, when OH^- ions are added to the crystal via diffusion, the observed signal is greatly decreased, presumably by some interaction between the Li^+ and OH^- ions. Many other ions suspected of being impurities in KBr were also added to the pure crystal but did not produce any observable PER signal. Since a few ppm of Li^+ are present in all crystals the addition of excess common impurities should lead to some signal if it arises from a Li^+ —impurity-ion complex. The absence of such a signal therefore supports our assertion that isolated lithium ions produce the PER signal.

Several unanswered questions certainly remain. Why is the fraction of active paraelectric centers so small? Why is the far-infrared mode so strong? How can this system be reconciled with recent theoretical results? Since even the $\langle 110 \rangle$ tunneling model is not rich enough to explain all the data, what kind of extensions or new models must be invoked to give at least a phenomenological understanding of the system?

The low effective concentration of paraelectric lithium centers and the apparently high concentra-

tion of infrared-active lithium centers conceivably are related. We have presented several arguments in Sec. IIC which support our hypothesis that it is the paraelectric centers that arise from isolated ions and not the infrared centers (assuming that isolated lithium cannot form two distinct centers). However, the small fraction of paraelectric centers is surprising and possibly results from the clumping of Li^+ ions into inactive pairs or more complex inactive groups as occurs for RbCl:Ag^+ . More importantly, in a recent study³⁰ of RbCl:Li^+ the signal intensity is linearly proportional to the Li^+ concentration up to a concentration of $10^{18}/\text{cm}^3$. Above this concentration, however, the signal intensity does *not* increase further, suggesting that above $10^{18}/\text{cm}^3$, some other lithium center forms—possibly pairs. If a similar effect also occurs in KBr:Li^+ (perhaps at a lower concentration level), but complicated by the experimental fact that traps such as OH^- exist for the Li^+ ion, then the low concentration of paraelectrically active centers is not too surprising. Support for this possibility is also found in a preliminary PER study of NaCl:Li^+ .⁴¹

If the paraelectric centers arise from isolated Li^+ ions then the infrared centers must be explained in terms of Li^+ pairs, Li^+ -complex centers, or possibly by assuming that *isolated Li^+ forms two (or more) different species*. The Li^+ pairs would give a center with D_{2h} symmetry while $\text{Li}^+:\text{X}^-$ or $\text{Li}^+:\text{Y}^+$ types of centers would have C_{4v} or C_{2v} symmetry. Some of the early ir experiments checked for the possibility that the Li^+ ion was frozen off center in a multiwell potential with C_{4v} , C_{3v} , or C_{2v} symmetry. The data were inconsistent with any of these symmetries, which suggests not only that such lithium-ion centers are *not* being frozen off center, but moreover that off-center centers probably do not produce the observed ir lines. (The D_{2h} symmetry was apparently not checked for specifically, but nevertheless appears to have been excluded.) For Li^+ pairs one might expect three ir modes plus some higher-frequency “optical” modes. Three ir modes are in fact observed, but the 16-cm^{-1} line is by far the strongest. Thus, although it might yet be possible to understand the ir results in terms of a Li^+ complex, the results to date suggest that two isolated Li^+ centers exist.

The theoretical situation for KBr:Li^+ is far from clear (see Sec. IIB) since trends in the theoretical calculations appear inconsistent with some experimental results.²² In addition to the KBr:Li^+ system, an exploratory PER study⁴¹ of

NaCl:Li⁺ indicates that NaCl:Li⁺ is also paraelectric. The particular host crystal considered in the present study, KBr, is a borderline *theoretical* case since for some choices of parameters, shallow off-center wells occur, while for others no off-center minima are found.^{21,23} It appears that the theoretical calculations are not yet precise enough to give reliable predictions in some situations.

Extensions of the standard tunneling models that might explain the complicated spectra found in KBr:Li⁺ must include additional zero-field splittings and hence additional states. For a simple off-center system, several possibilities exist consistent with the cubic symmetry. Each requires a much more convoluted potential energy surface than is envisaged for the standard models and thus requires that distant neighbors have an important influence on the potential. In the past, the requirement for a highly convoluted energy surface has been an argument against these more complicated models; however, the present data clearly indicates the need for such further theoretical development.

VII. CONCLUSIONS

We have presented an extensive PER study of KBr:⁷Li⁺ and KBr:⁶Li⁺ over a wide range of microwave frequencies. The spectra are unusual in many ways—very large zero-field splittings, more energy levels than one expects for the simple tunneling models and an apparently low concentration of active centers. The understanding of this unique paraelectric system is further complicated by the observation that some other impurity ions, such as OH⁻, can suppress the PER signal and that quenching the samples can greatly increase the number of active paraelectric centers. In addition, a large isotope shift and a consistent dipole moment are observed when ⁶Li⁺ is substituted for ⁷Li⁺.

Our data strongly suggests that the paraelectric behavior arises from isolated Li⁺ ions in the crystal. We analyzed the data using the standard tunneling models and also considered a number of simple Li⁺—impurity-ion complexes. The latter generally had less structure than the simple tunneling models and therefore not enough transitions to explain our complicated data. Even the $\langle 110 \rangle$ model could not explain all the data, although it could fit a few lines in each orientation very well.

The importance of the Li⁺ systems lies in the fact that KCl:Li⁺ is considered a model system for off-center paraelectric behavior. The Li⁺ ion is

small, much less polarizable than other larger off-center ions such as Cu⁺ and Ag⁺; consequently, it has been assumed that the Li⁺ centers in the alkali halides constitute an ideal set for investigating on-center and off-center behavior. The present study, plus the observation of PER in NaCl:Li⁺ and the signal saturation effect at low concentrations in RbCl:Li⁺, indicate that even for the Li⁺ ion the paraelectric behavior is very difficult to predict theoretically. Further study is needed to understand the relationship between the paraelectric-paraelastic center and the nonparaelectric center observed in far-infrared studies.

ACKNOWLEDGMENTS

We thank W. Kelly for his help constructing and running the spectrometer, and for his comments and insights. We also thank J. Rudnick, G. Gaspari, F. Lüty, G. Dick, and A. Sievers for helpful discussions over the course of this work. This project was supported in part by a grant from the National Science Foundation.

APPENDIX A: LITHIUM COMPLEX MODELS

1. Li⁺:X⁻ model with Li⁺ tunneling in a single plane

We assume that Li⁺ goes off center as a result of the presence of a nearest-neighbor X⁻ ion which produces a C_{4v} axis in the crystal. Two distinct complexes might occur—Li⁺ off center along

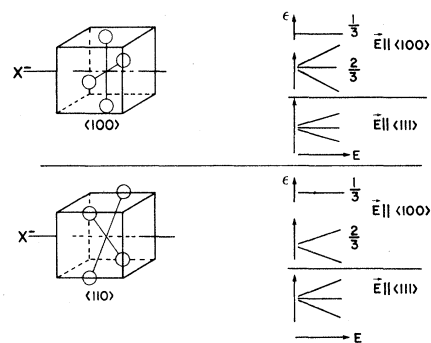


FIG. 19. Schematic representation of the Li⁺:X⁻ model with off-center wells (indicated by circles) orientated along either the $\langle 100 \rangle$ or $\langle 110 \rangle$ directions. For $\vec{E} \parallel \langle 100 \rangle$, $\frac{1}{3}$ of the centers have E parallel to the C_{4v} axis and show no splitting. Splittings for $\vec{E} \parallel \langle 100 \rangle$ and $\vec{E} \parallel \langle 111 \rangle$ are indicated for other orientations of the C_{4v} axis.

the four $\langle 100 \rangle$ directions or along the four $\langle 110 \rangle$ directions as shown in Fig. 19.

For an applied \vec{E} field along $\langle 100 \rangle$, $\frac{1}{3}$ of the complexes with the $\text{Li}^+ \cdot \text{X}^-$ axis parallel or antiparallel to \vec{E} will have no change in energy. For the other C_{4v} axes, the energy levels will be split by the $-\vec{p} \cdot \vec{E}$ interaction as shown schematically in Fig. 19. The splittings for $\vec{E} \parallel \langle 111 \rangle$ are also shown.

For each case the zero-field energy levels form two singlets and a doublet. Consequently, at most, three zero-field splittings should be observed, and only two may be independent.

2. $\text{Li}^+ : \text{Y}^+$ model with Li^+ tunneling in a single plane

A positively charged impurity Y^+ would occupy a second-nearest-neighbor site and produce a C_{2v} axis in the crystal. Three simple complexes might occur with the Li^+ off center in a direction perpendicular to a given C_{2v} axis—the Li^+ might occupy two $\langle 100 \rangle$, two $\langle 110 \rangle$, or possibly four $\langle 111 \rangle$ off-center sites as shown in Fig. 20. The first two cases produce only a pair of levels and consequently only one ZFS while the latter has four separate nondegenerate states (and three independent ZFS's) in the absence of external fields. In all cases $\vec{E} \parallel \langle 100 \rangle$ will produce only one slope in a plot of line position versus frequency.

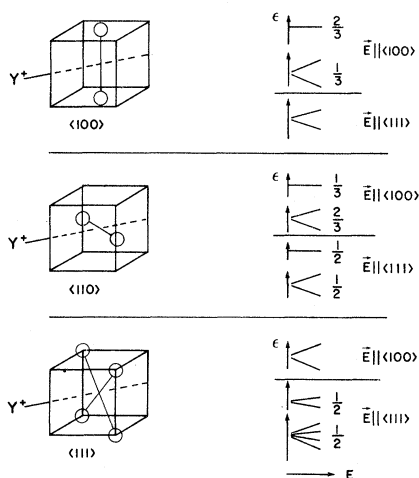


FIG. 20. Schematic representation for the $\text{Li}^+ : \text{Y}^+$ model in which off-center potential wells along $\langle 100 \rangle$, $\langle 110 \rangle$, or $\langle 111 \rangle$ directions are induced perpendicular to the C_{2v} axis. Energy levels for $\vec{E} \parallel \langle 100 \rangle$ and $\vec{E} \parallel \langle 111 \rangle$ are given for each case.

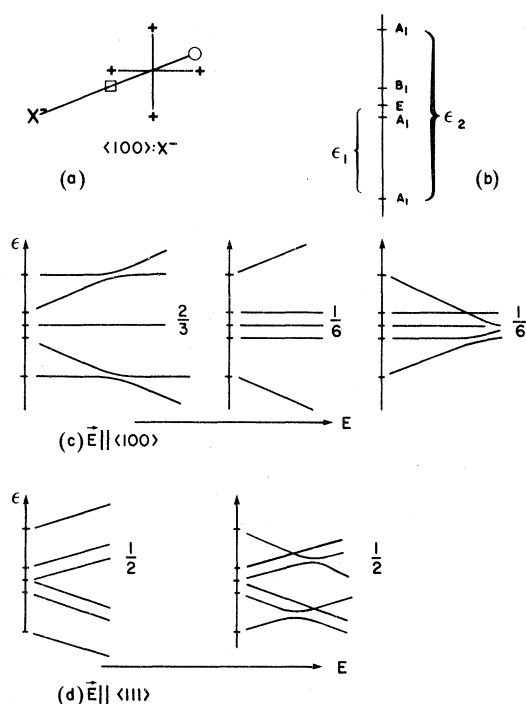


FIG. 21. $\langle 100 \rangle : \text{X}^-$ model. It is assumed that the Li^+ ion moves off center as a result of the X^- anion, along the $\langle 100 \rangle$ crystal directions. Three planes of inequivalent off-center ions are found, denoted by a square, crosses, or a circle. Energies ϵ_1 and ϵ_2 are the energy splittings between these planes. In the presence of an electric field, the energy-level splittings depend on the relative orientation of the C_{4v} axis and the electric field and give rise to different splittings for different orientations. Fractions $\frac{2}{3}$, $\frac{1}{6}$, etc., indicate the fraction of centers with that particular energy-level diagram.

One special case of such a complex is a $\text{Li}^+ : \text{Li}^+$ pair. Here both Li^+ ions may be off center and the number of states is doubled. In addition, the dipole-dipole interaction will further split the zero-field energies. However, even with these added complications, only *one* slope on a line position versus frequency plot is expected.

3. $\text{Li}^+ : \text{X}^-$ model with Li^+ tunneling in several planes

Here we assume that the presence of an impurity anion X^- provides a strong C_{4v} perturbation to the crystal and that the resulting off-center positions can be viewed as one of the simple tunneling models in the presence of some C_{4v} interaction.

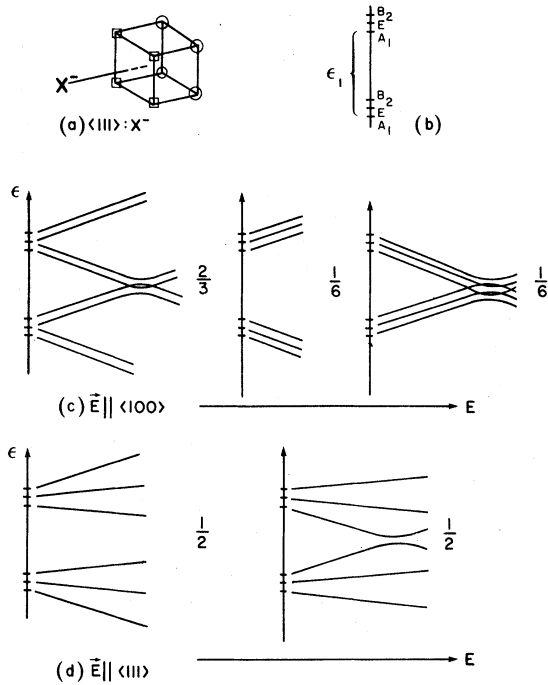


FIG. 22. $\langle 111 \rangle : X^-$ model. This is similar to Fig. 21 but has the off-center wells along $\langle 111 \rangle$ directions instead of $\langle 100 \rangle$ directions, forming two planes of inequivalent wells—squares and circles. ϵ_1 is the energy splitting between these two planes.

We emphasize that in this model it is the *presence* of the C_{4v} interaction that *forces* the off-center displacement. Consequently we do not consider small perturbations of a simple off-center system here, and we assume that the C_{4v} perturbation is larger than the tunneling parameters, but not necessarily larger than the $-\vec{p} \cdot \vec{E}$ interaction with an external field. Then the off-center positions can be grouped into planes perpendicular to the C_{4v} axis. We assume for *simplicity* that the off-center position (i.e., the off-center dipole) is the same in each plane. The energy of each plane (neglecting tunneling) ϵ_1, ϵ_2 , etc., is determined by the C_{4v} perturbation.

(i) $\langle 100 \rangle : X^-$ model. In this case, three groups of off-center positions exist as indicated by a circle, a square, and crosses on Fig. 21(a). We take the energy of the off-center position nearest the X^- ion as zero and let the energies of the remaining planes be ϵ_1 and ϵ_2 . Then the zero-field splittings will be grouped about energies ϵ_1, ϵ_2 , and $\epsilon_2 - \epsilon_1$ as indicated in Fig. 21(b). Including tunneling splittings, at most four independent ZFS's are possible.

For $\vec{E} \parallel \langle 100 \rangle$, $\frac{2}{3}$ of these centers will have \vec{E}_{dc} perpendicular to the C_{4v} axis, and if η is dominant, several backward transitions should occur, as well

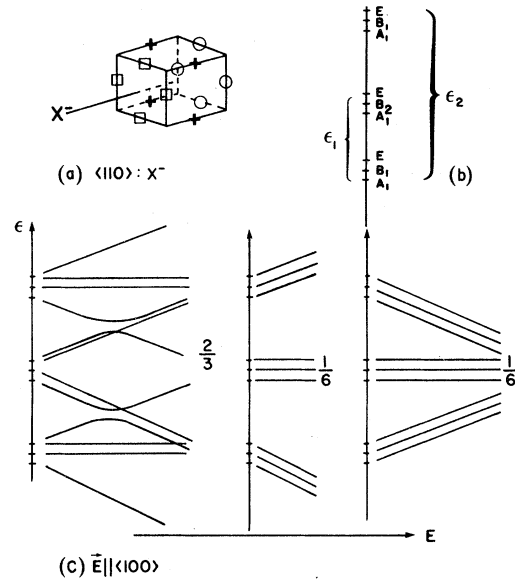


FIG. 23. $\langle 110 \rangle : X^-$ model. This is similar to Fig. 21 but has the off-center wells along $\langle 110 \rangle$ directions instead of $\langle 100 \rangle$ directions, forming three planes of inequivalent wells. ϵ_1 and ϵ_2 again represent the energy splittings between these wells.

as several “level crossings”. Of the remaining $\frac{1}{3}$ of the centers, half of them will have the top and bottom levels diverging with \vec{E}_{dc} while the other half will have them converging [Fig. 21(c)]. For the converging case μ (180° tunneling) will allow additional backward lines.

For $\vec{E} \parallel \langle 111 \rangle$ many possibilities also exist. One-half of the centers should produce backward lines and some level crossings. However, for all cases, only *one* slope will be observed on a line position versus frequency plot. (Backwards lines would have the negative of this slope.)

(ii) $\langle 111 \rangle : X^-$ model. In this case, two planes of off-center positions occur as indicated by squares and circles in Fig. 22(a). There are six energy levels and five independent ZFS's. ϵ_1 is the energy difference for the two planes.

For $\vec{E} \parallel \langle 100 \rangle$, $\frac{2}{3}$ of the centers will have \vec{E}_{dc} perpendicular to the C_{4v} axis, while $\frac{1}{6}$ are parallel and $\frac{1}{6}$ antiparallel to this axis [Fig. 22(c)]. The first and last cases should produce backward lines and in all cases only one magnitude of slope should be observed.

For $\vec{E} \parallel \langle 111 \rangle$, several different slopes are possible and some backward lines are expected if η or ν are important tunneling parameters.

(iii) $\langle 110 \rangle : X^-$ model. Here there are three planes of off-center positions with four potential wells in each plane [Fig. 23(a)]. Including tunnel-

ing, each group splits into three distinct energy levels (one is a doublet in each case) giving nine different energy levels [Fig. 23(b)] and many different ZFS's. An important characteristic of this model

is that for *any* choice of tunneling parameters, backwards lines are expected for both $\bar{E}||\langle 100 \rangle$ and $\bar{E}||\langle 111 \rangle$.

-
- *Present address: The Center for Theology and the Natural Sciences, 2465 Le Conte Avenue, Berkeley, CA 94709.
- ¹R. A. Herendeen and R. H. Silsbee, *Phys. Rev.* **188**, 645 (1969).
 - ²For a review of paraelectric tunneling systems, see F. Bridges, *Crit. Rev. Solid State Sci.* **5**, 1 (1975); V. Narayanamurti and R. O. Pohl, *Rev. Mod. Phys.* **42**, 201 (1970).
 - ³F. C. Baumann, J. P. Harrison, R. O. Pohl, and W. D. Steward, *Phys. Rev.* **159**, 691 (1967).
 - ⁴J. P. Harrison, P. P. Peressini, and R. O. Pohl, *Phys. Rev.* **171**, 1037 (1968).
 - ⁵G. Lombardo and R. O. Pohl, *Phys. Rev. Lett.* **15**, 291 (1965).
 - ⁶S. Kapphan, Ph.D. thesis, University of Utah, 1970 (unpublished).
 - ⁷A. J. Sievers and S. Takeno, *Phys. Rev.* **140**, A1030 (1965).
 - ⁸R. D. Kirby, I. G. Nolt, R. W. Alexander, and A. J. Sievers, *Phys. Rev.* **168**, 1057 (1968).
 - ⁹R. D. Kirby and A. J. Sievers, *Solid State Commun.* **6**, 613 (1968).
 - ¹⁰I. G. Nolt and A. J. Sievers, *Phys. Rev. Lett.* **16**, 1103 (1966); *Phys. Rev.* **174**, 1004 (1968).
 - ¹¹A. M. Kahan, Ph.D. thesis, Cornell University, 1973 (unpublished).
 - ¹²A. M. Kahan, M. Patterson, and A. J. Sievers, *Phys. Rev. B* **14**, 5422 (1976).
 - ¹³F. Bridges, *Bull. Am. Phys. Soc.* **19**, 328 (1974).
 - ¹⁴F. Bridges and R. J. Russell, *Solid State Commun.* **21**, 1011 (1977).
 - ¹⁵M. Gomez, S. P. Bowen, and J. A. Krumhansl, *Phys. Rev.* **153**, 1009 (1967).
 - ¹⁶H. Shore, *Phys. Rev.* **151**, 570 (1966).
 - ¹⁷P. Sauer, O. Schirmer, and J. Schneider, *Phys. Status Solidi* **16**, 79 (1966).
 - ¹⁸R. J. Russell, preceding paper, *Phys. Rev. B* **26**, 3376 (1982).
 - ¹⁹R. J. Quigly and T. P. Das, *Phys. Rev.* **164**, 1185 (1967); **177**, 1340 (1969).
 - ²⁰W. D. Wilson, R. D. Hatcher, G. J. Dienes, and R. Smoluchowski, *Phys. Rev.* **161**, 888 (1967); **184**, 844 (1969).
 - ²¹C. R. A. Catlow, K. M. Diller, M. J. Norgett, J. Corish, B. M. C. Parker, and P. W. M. Jacobs, *Phys. Rev. B* **18**, 2739 (1978).
 - ²²U. Holland and F. Lüty, *Phys. Rev. B* **19**, 4298 (1979).
 - ²³M. J. L. Sangster, *J. Phys. C* **13**, 5279 (1980).
 - ²⁴F. Bridges, *Rev. Sci. Instrum.* **45** (1974).
 - ²⁵W. M. Kelly and F. Bridges, *Phys. Rev. B* **18**, 4606 (1978).
 - ²⁶F. Bridges, *Phys. Rev. B* **5**, 3321 (1972).
 - ²⁷The high-slope line 5 in the $\langle 111 \rangle$ data, with a relatively small zero-field splitting, is a very unusual feature of the data since high-slope lines usually have one of the largest zero-field splittings.
 - ²⁸Line 4 appears to have the same slope as lines 2, 3, and 5 and in this boule has a strength comparable to line 2. However, it may correspond to the questionable line in the $\langle 100 \rangle$ data and therefore may be spurious.
 - ²⁹F. Holuj and F. Bridges, *Phys. Rev. B* **20**, 3578 (1979).
 - ³⁰K. Thorner and F. Lüty, *Phys. Status Solidi B* **90**, 277 (1978).
 - ³¹F. Lüty (private communication).
 - ³²R. J. Russell, Ph.D. thesis, 1978 (unpublished).
 - ³³The variation in relative intensity was usually less than a factor of 2 and is expected when broad overlapping lines must be decomposed. For very broad lines, shifts in the line positions appeared, particularly at low fields.
 - ³⁴F. Bridges, *Phys. Rev. B* **23**, 453 (1981); R. J. Russell, *Bull. Am. Phys. Soc.* **26**, 30 (1981).
 - ³⁵R. V. Jimenez and F. Lüty, *Phys. Rev. B* **12**, 1531 (1975).
 - ³⁶The thermal-conductivity resonances (Ref. 3) were fit to Lorentzian line shapes, with the integrated intensity proportional to the dopant concentration N and a scattering strength A . For KBr:Li^+ , A was a factor of 300 lower than expected. If, however, only 0.3% of the added Li were active in this sample, then the empirical value of A would be consistent with other tunneling systems.
 - ³⁷A. J. Sievers (private communication).
 - ³⁸B. Clayman (private communication).
 - ³⁹H. Ohkura, Y. Mori, M. Matsuoka, T. Watanabe, and A. Satoh, *Suppl. Prog. Theor. Phys.* **57**, 68 (1975).
 - ⁴⁰W. Zoller and F. Bridges, *Phys. Rev. B* **24**, 4796 (1981).
 - ⁴¹R. J. Russell and F. Bridges, *Bull. Am. Phys. Soc.* **23**, 18 (1978). In these experiments, a paraelectric center was found that is similar to KBr:Li^+ —large zero-field splittings and a large isotope shift.